國 立 交 通 大 學

電子工程學系 電子研究所碩士班

碩 士 論 文

射頻積體電路之基板雜訊耦合分析及模型化

Analysis and Modeling of Substrate Noise Coupling in RFICs

研 究 生：蔡坤宏

指導教授：郭建男 教授

中 華 民 國 九十四 年 七 月

射頻積體電路之基板雜訊耦合分析及模型化

Analysis and Modeling of Substrate Noise Coupling in RFICs

研 究 生：蔡坤宏　　　　　Student：Kun-Hung Tsai

指導教授：郭建男　　　　　Advisor：Chien-Nan Kuo

國 立 交 通 大 學

電子工程學系 電子研究所碩士班

碩 士 論 文

A Thesis
Submitted to Department of Electronics Engineering & Institute of Electronics
College of Electrical Engineering and Computer Science
National Chiao Tung University
In Partial Fulfillment of the Requirements
For the Degree of
Master
In
Electronic Engineering
July 2005
Hsinchu, Taiwan, Republic of China

中 華 民 國 九十四 年 七 月

射頻積體電路之基板雜訊耦合分析及模型化

學生：蔡 坤 宏　　　　　　　　　　指導教授：郭 建 男 教授

國立交通大學

電子工程學系 電子研究所碩士班

摘要

在本論文中，我們由頻域的觀點來探討射頻積體電路中，元件因耗損性矽基板所產生的雜訊耦合效應。對此，論文分別針對射頻被動元件(電感)及電晶體(MOSFET)所生的雜訊經由矽基板傳導的現象，作分析及模型化。

被動元件部分，我們製作二種不同擺放方法的電感對，並改變其距離，觀察電感所生的基板雜訊耦合效應對距離變化的情況，同時，亦觀察電感受到雜訊耦合後，電感本身特性改變的情形。之後，再由模擬及量測的相互驗證，提出雜訊耦合的等效電路模型，描述基板雜訊的行為。

在電晶體部分，我們可以知道金氧半電晶體的源、汲二極因 P-N 接面的關係會產生寄生的空乏電容，此一寄生電容會將高頻的雜訊耦

合到基板，而使雜訊影響電路工作的準確性。針對此點，我們設計測試鍵來量測高頻雜訊因接面電容耦合到基板的現象。在測試鍵中，我們將 P-Well 及 N-Well 中分別打入 N-diffusion 及 P-diffusion 形成空乏電容，同時調整 diffusion 的距離，並量測雙埠(Two-port)的散射參數(S-parameter)，得知高頻雜訊對距離變化的情況。

最後，這些量測結果及等效模型，將提供給電路設計者，期能經由這些資訊，可讓高頻電路設計更有效率。

Analysis and Modeling of Substrate Noise Coupling in RFICs

Student: Kun-Hung Tsai Advisor: Prof. Chien-Nan Kuo

Department of Electronics Engineering & Institute of Electronics

National Chiao.Tung University

ABSTRACT

In this thesis, the substrate noise coupling effect in the lossy silicon substrate is investigated from the aspect of frequency domain. Therefore, the coupling effect produced by the passive device and MOSFET is also analyzed and modeled.

In the part of passive device, two types of inductor pairs are fabricated and the distance between the inductor pairs is varied to observe the substrate coupling effect with regards to the different distance. Furthermore, the characteristic of inductor changed by coupling effect is also studied. Then, from the measurement and simulation results, an equivalent circuit model of substrate noise coupling effect in the inductor pairs is proposed, too.

In the part of MOS transistor, we study the noise coupling from the source and drain depletion capacitance (formed by the P-N junction). However, these parasitic capacitances would couple the RF noise to substrate and then degrade the performance of RF circuit. From the point of view, the testkey is designed to measure the phenomenon of RF noise coupling effect. In the testkey, the N-diffusion and P-diffusion regions are formed inside the P-well and N-well then induce the junction capacitance. Next, the distance of two diffusion regions is changed and measured the

S-parameters to obtain the noise coupling effect for the varying different distance.

Finally, these measurement results and equivalent circuit model would provide to circuit designers and hope the information would let the RF circuit design procedure be more efficient.

誌謝

首先要感謝我的指導教授郭建男博士在這二年來給我的指導，老師豐富的學識及治學嚴謹的態度，讓我在碩士班的修業過程中，獲益良多，在此向老師獻上最深的敬意。

感謝一起在實驗室共患難的學長，同學及學弟妹們。同期的維嘉及仰鵬，在我遇到困難時，不吝伸出援手，拉我一把，讓我在能順利的渡過。實驗室的大學長，昶綜，更是在研究上時常提點我，讓我的研究能夠突破難關。同時，也要謝謝凱哥在製程上的幫忙，以及子倫與 NDL 的黃國威、邱佳松、卓銘祥先生在量測上的協助，由於他們的鼎力相助，讓我有了畢業的機會，當然，達道與岱原也為實驗室注入了活力，讓我在研究苦悶之餘，心情能夠獲抒解。

最後，還要感謝我的父母及鄒佩真小姐，他們是我心情的避風港，不管我遇到了什麼問題，他們總是默默地支持我，給我鼓勵，讓我萌生勇氣，一步一步地走完這段求學路。當然，也還有很多認識或不認識的朋友，給了我很多幫忙，在此一併謝過。

蔡坤宏

九十四年七月

CONTENTS

TABLE CAPTIONS

FIGURE CAPTIONS

CHAPTER 1

Introduction

1.1 Motivation

In the recent years, due to the great enhancement of CMOS technology, the application of radio frequency integrated circuits (RFICs) in CMOS technology is possible. Moreover, the advanced CMOS technology can also integrate digital circuits with analog and RF circuits in a single chip. As a result, the concept of "System On a Chip (SOC)" comes after the advanced CMOS technology. However, there are still some difficulties in the integration of these circuit blocks, such as the substrate noise coupling effect, quality of passive components, [1], etc. The most urgent issue is the substrate noise coupling effect. As everyone knows, the silicon substrate is not a perfect insulator; nonetheless, it may deliver the noise (switching MOS noise, ground bounce, etc.) from the digital part to analog or RF part. Those unwanted signals will degrade the performance of the sensitive circuit greatly.

Besides, it can be found that the employment of spiral inductor is very popular in RF circuits, such as LNA, VCO, mixer, and many other circuits. When the operation frequency is increased (up to several giga Hertz), the coupling effect of inductor to substrate or inductor to adjacent inductor is significant. To reduce the coupling effect between inductors, some methodologies like the ground shield or guard ring is often used for preventing the coupling effect. However, these methodologies degrade the inductor performance thereby presenting a trade-off in the device design.

In the thesis, the analysis for coupling effects of MOS and inductors from the aspect of frequency domain is presented and a correspondent model is proposed to characterize the substrate noise coupling behavior in the lossy substrate accordingly.

1.2 Thesis organization

In the chapter 2 of the thesis, we introduce some substrate noise coupling mechanisms, including the switching transients in digital MOS circuits and ground bounce in the switching MOS and digital power lines. In addition, the electromagnetic coupling effect of inductor in the giga frequency range is also shown in this chapter.

The substrate coupling mechanisms that we want to investigate are presented in chapter 3 and chapter 4. In chapter 3, the simulation and measurement results of electromagnetic coupling between two adjacent inductors are presented. Furthermore, an equivalent circuit model is established to describe the coupling phenomenon in the lossy silicon substrate. In chapter 4, the substrate noise coupled effects from the source and drain parasitic capacitance in TSMC 0.18 um CMOS process are discussed, and the measurement results are presented as well.

In the last chapter, a conclusion of the thesis is made and the future work on the exploration of the substrate noise phenomena is thereof addressed.

CHAPTER 2

Basic Concepts of the Coupling Effect in Silicon Substrate

In this chapter, the basic concepts of noise coupling in silicon substrate are illustrated. The noise induced from a digital circuit block is presented in Section 2.1. Section 2.2 gives some information about the electromagnetic coupling effect in RF integrated circuits.

2.1 Noise coupling in digital circuit

As everyone knows, all currents that injected into the substrate will cause fluctuations of substrate voltage. These fluctuations are called the substrate noise and caused by switching or noisy signal in digital circuits. In the section, the noise coupling mechanisms are divided into three parts. The first part is the noise produced by the digital power supply and bond wire parisitics. The second part is the capacitive coupling effect from source-drain node to substrate. And the last is due to the impact ionization of MOSFET device.

The first one is due to the *di/dt* noise [2] (or delta I noise) and resistive voltage drops made by the inductance and resistance in the power supply connected to the chip. As shown in Fig. 2.1, the parasitic inductance of the bond wire connected to power supply is the main factor that causes the *di/dt* noise. Besides, the combination of the inductance in the power supply and capacitor in bonding pad will cause the ringing of the power supply voltage. These effects made by power lines are called ground bounce, too.

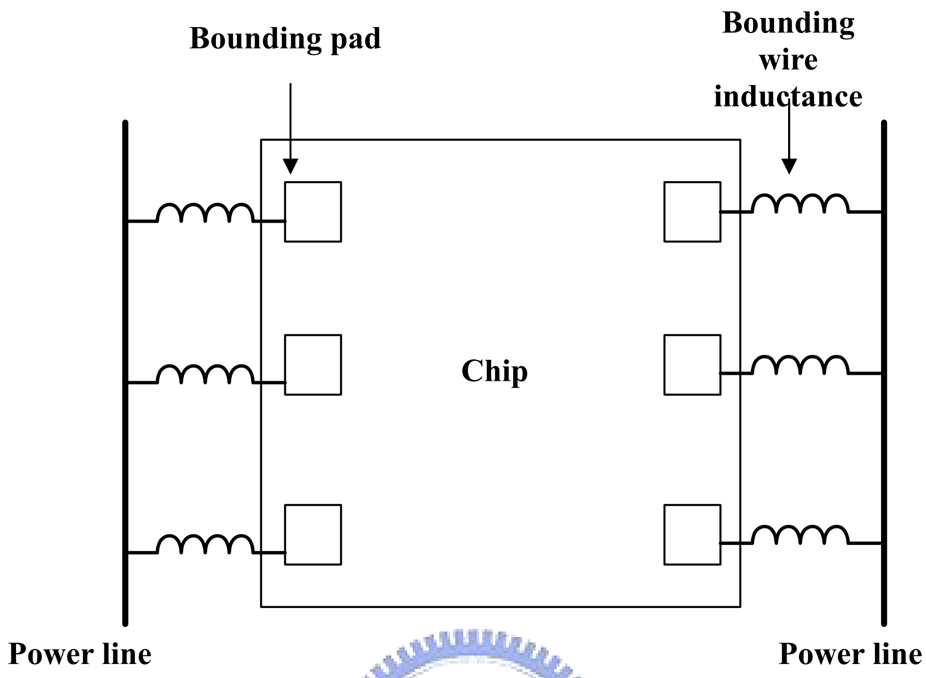

Fig. 2.1 Chip parasitic in a package.

The second source of substrate noise is the capacitive coupling from drain or source node of the MOS transistor. As it is shown in Fig. 2.2, a digital switching device induces currents to substrate through the depletion capacitances of the p-n junction. Therefore, the amount of capacitive coupling noise will be larger as the transient time becomes faster. On the other hand, the parasitic capacitance induced by the interconnect is also added to the junction capacitance of source-drain and then causes the more severe coupling effect.

The third origin of substrate noise is the impact ionization. The importance of noise caused by impact ionization depends on the CMOS technology. When the CMOS technology goes to deep submicron level, the impact-ionization current have gained significance. In deep submicron device, hot carrier effects become a major source of noise injection [3].

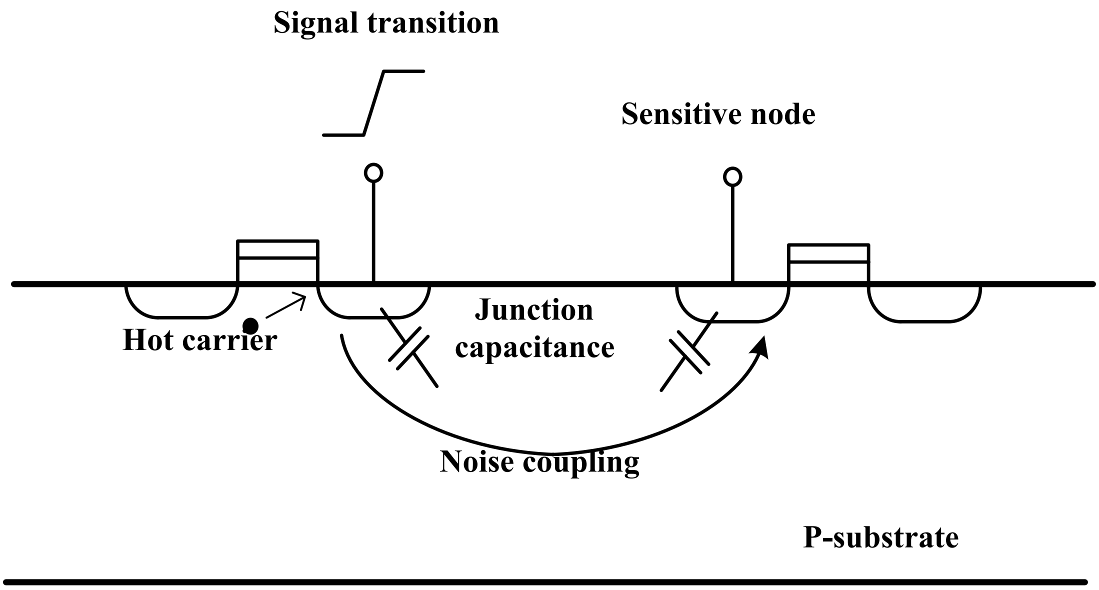

Fig. 2.2 Noise coupling mechanisms from substrate.

2.2 Electromagnetic coupling in Si substrate

From Section 1.1, because of the concept of SOC, the integration of RF circuits in CMOS process is actively pursued in an effort to increase functionality and reduce cost. For the giga hertz frequency range, the electromagnetic coupling between RF circuit blocks through the lossy substrate is a concern. For example, the large RF signal power produced by a power amplifier will pass through the substrate and then affect the other sensitive circuit. Moreover, the on-chip inductors are often used in RF circuit designs, such as the low noise amplifier, band-pass filter, and mixer. As shown in Fig. 2.3 and Fig. 2.4, the electromagnetic coupling between two closely placed interconnects or inductors is also a way that induces the electromagnetic coupling in RFICs (Fig. 2.3). Therefore, if high-frequency coupling effects are not taken into account, the RF circuit performance will be degraded by these unwanted coupling effects.

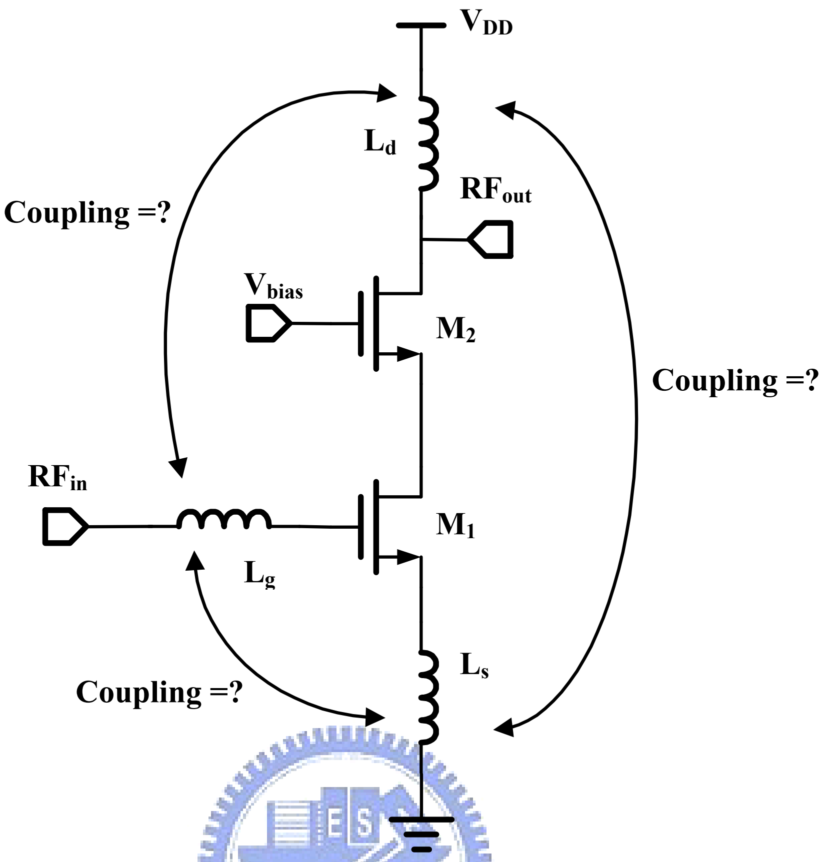

Fig. 2.3 Low noise amplifier suffering from the on-chip inductor coupling effect.

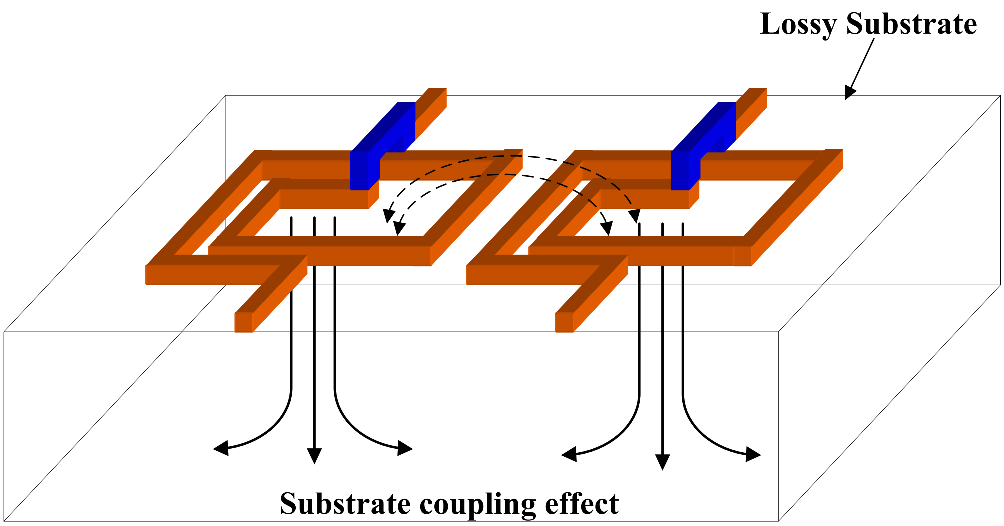

Fig. 2.4 Coupling effect of two adjacent inductors.

CHAPTER 3

Investigation of RF Spiral Inductor's Coupling Effects in Lossy Substrate

In this chapter, the coupling effects of two adjacent coplanar spiral inductors are investigated. First, the manufacturing process of the inductor is provided by NCTU Nano Facility Center (國立交通大學奈米中心). The process is different from the standard CMOS process utilized by TSMC or UMC. Second, the inductor coupling structure is proposed and the simulation results are shown. Finally, the measurement data and proposed model of inductor coupling effect are also obtained.

3.1 Design consideration of a single inductor

3.1.1 The fabrication process of the inductor

As mention before, the process is provided by NCTU Nano Facility Center; the process is quite different from the commercial process, such as TSMC or UMC standard CMOS process. The wafer is the 4 inch P-type doped wafer with a substrate resistivity of 21~23 Ω/cm. In order to get a good electrical performance, a sandwiched type membrane consisted of 0.7um thermal oxide, 0.7um LPCVD Si_3N_4, and 0.7um TEOS oxide is employed ($SiO_2$0.7um/$Si_3N_4$0.7um/$SiO_2$0.7um, [4]). The cross-section view of these oxide layers are shown in Fig. 3.1 and the advantages of the proposed sandwiched structure are illustrated as the follows:

(1) Low dielectric loss: Because of the low conductivity and loss tangent properties, these dielectric layers have the low electromagnetic energy loss.

(2) Stress issue: The Young's modulus of Si_3N_4 is five times larger than that of SiO_2 (Table 3.1); the Si_3N_4 layer has the much higher residual stress with the silicon substrate in comparison with SiO_2. However, if proposed sandwiched structure is utilized, the nitride stress can be effectively released by using the double oxide layers.

Table 3.1 Young's modulus.

Material / *Parameter*	***SiO2***	***Si_3N_4***
Young's modulus (GPa)	73	310

The copper is utilized to form the metal strip of inductor. The metal is deposited above oxide layer by using electroplating method with the H_2SO_4 plating bath and the copper anode. The total reaction of the plating procedure can be written as:

$$Cu^{2+} + 2e^{-} \rightarrow Cu \qquad (3.1)$$

The setup of the electroplating method is presented in Fig. 3.2.

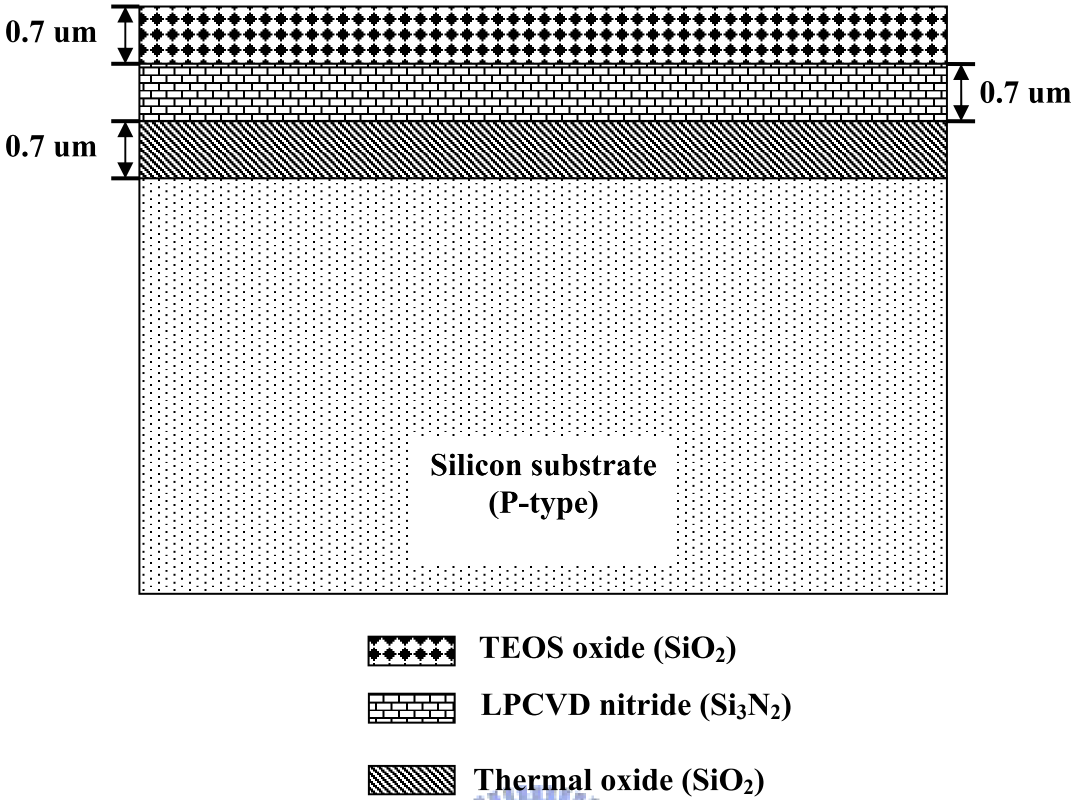

Fig. 3.1 The cross-section view of the sandwich membrane.

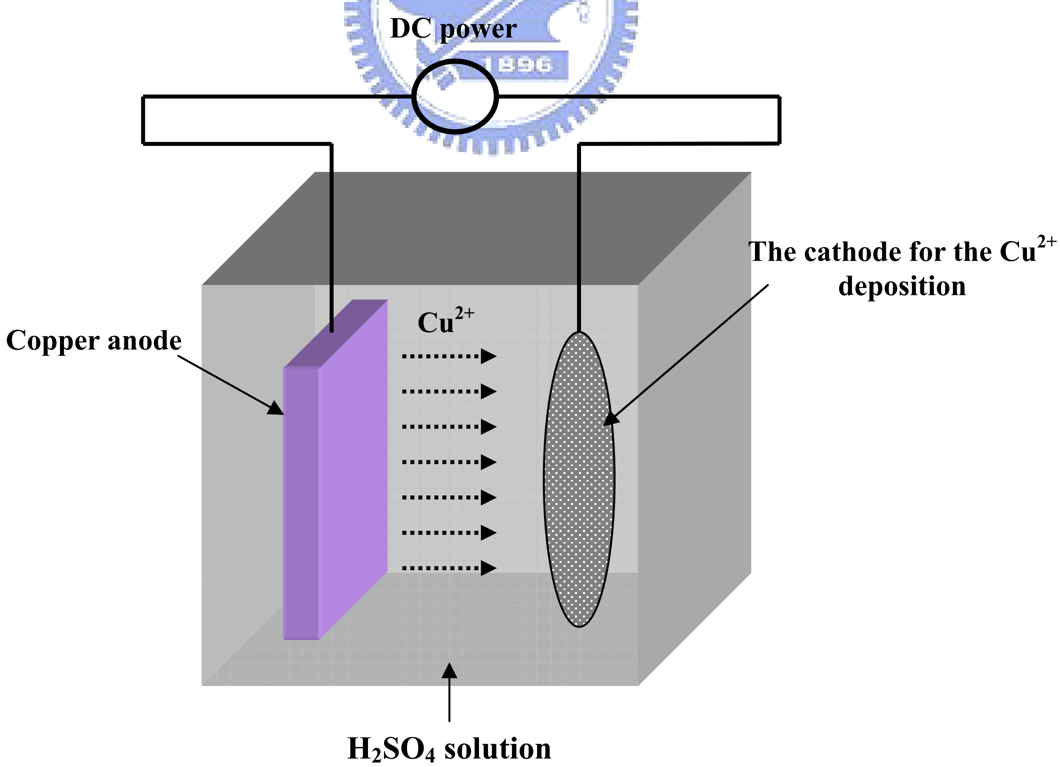

Fig. 3.2 The setup of the electroplating method.

3.1.2 Specification of spiral inductor

The size of the spiral inductor is shown in Fig. 3.3. Due to the process limitation, the space between two adjacent metal lines is 5um, the metal width and thickness are 15 um and 5 um, respectively. And the inner radius of the inductor is 60um. The graphical structure and design specifications are given in Fig. 3.3.

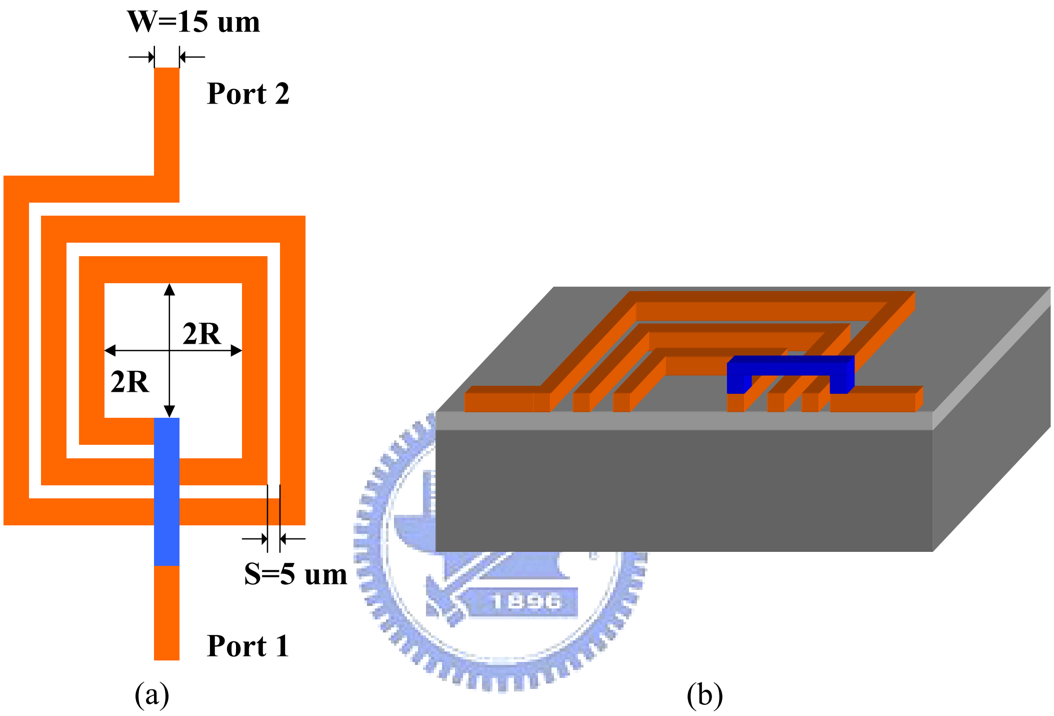

Fig. 3.3 Structure drawing of the inductor: (a) Top view. (b) Cross-section view.

3.2 Measurement results and modeling of a single inductor

3.2.1 Measurement setup

The S-parameters of a spiral inductor is measured by Agilent 8364B network analyzer and two GSG coplanar probes. The measurement setup is illustrated in Fig. 3.4 and the frequency range of measurement is from 0.1 GHz to 30 GHz.

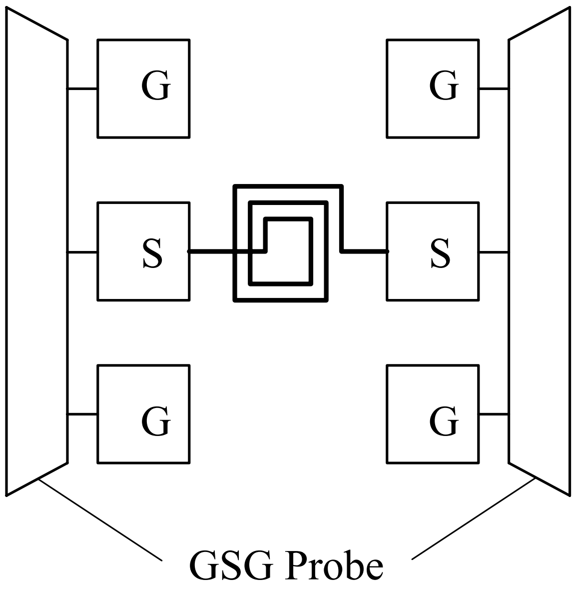

Fig. 3.4 Measurement setup of the single inductor.

3.2.2 De-embedding procedure

To obtain a precise measurement of the inductor S-parameter, the paracitic effects of GSG pad are needed to be removed. Therefore, a process called "de-embedding" should be done after the complete two-port calibration. A de-embedding procedure that contains the open circuit and short circuit method (OSD) [5] is used in the measurement of inductor S-parameter. The paracitics of GSG pads are illustrated in Fig. 3.5; the pad parasitic is lumped as y_p and the parasitic due to pad and probe tip interface discontinuity is modeled as Z_i. After the parasitics are defined, the Z_i and y_p are extracted by the short and open test pattern. Therefore, the S-parameters of single inductor without pad parasitics can be obtained by transmission matrix operation. The de-embedding procedure can be written as the follows:

$$Z_i = Z_{in,short}$$

$$y_p = \frac{1}{\left(Z_{in,open} - Z_{in,short}\right)}$$

The transmission matrix (T) of DUT (Device Under Test) can be derived [6]:

$$[\mathrm{T}]_{Z_i} = \begin{bmatrix} 1 & Z_i \\ 0 & 1 \end{bmatrix}, [T]_{y_p} = \begin{bmatrix} 1 & 0 \\ y_p & 1 \end{bmatrix}$$

$$\Rightarrow [T]_{measure} = [T]_{Z_i} [T]_{y_p} [T]_{DUT} [T]_{y_p} [T]_{Z_i}$$

$$\Rightarrow [T]_{DUT} = [T]_{y_p}^{-1} [T]_{Z_i}^{-1} [T]_{measure} [T]_{Z_i}^{-1} [T]_{y_p}^{-1}, \, and \; [T]_{dut} = \begin{bmatrix} A & B \\ C & D \end{bmatrix}$$

Therefore, the S-parameters of the DUT can be obtained from $[T]_{DUT}$

$$[S]_{DUT} = \begin{bmatrix} S_{11} & S_{12} \\ S_{21} & S_{22} \end{bmatrix},$$

Where

$$S_{11} = \frac{A + B/Z_0 - CZ_0 - D}{A + B/50 + CZ_0 + D} \quad , \quad S_{12} = \frac{2(AD - BC)}{A + B/Z_0 + CZ_0 + D}$$

$$S_{21} = \frac{2}{A + B/Z_0 + CZ_0 + D} \quad , \quad S_{22} = \frac{-A + B/Z_0 - CZ_0 + D}{A + B/50 + CZ_0 + D}, \text{and } Z_0 = 50\,\Omega$$

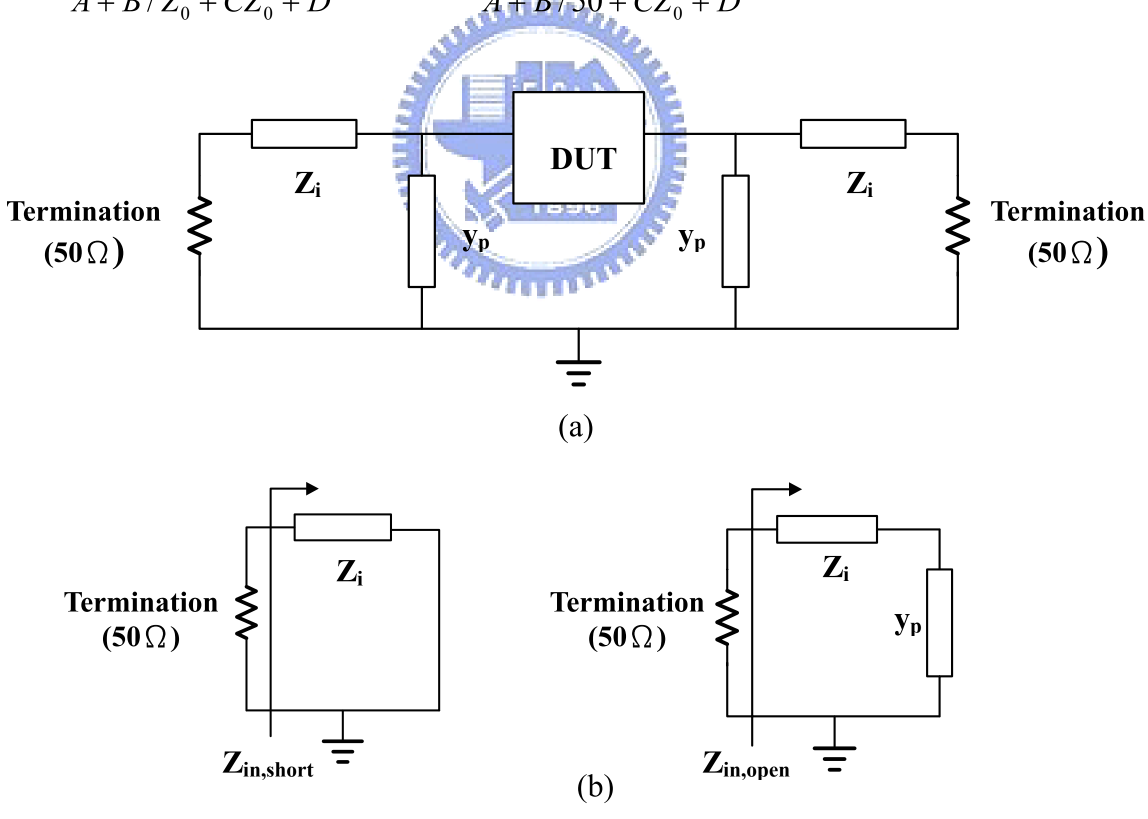

Fig. 3.5 Parasitic of GSG pad and pad parastics extraction. (a) The equivalent circuit model of pad parasitic. (b) The extraction method of pad parasitic.

3.2.3 Measurement results and equivalent circuit model of spiral inductor

In reference to the micrograph of a 3.5 turns spiral inductor as shown in Fig.3.6 and the comparisons between measurement (Mea.) and simulation (Sim.) results using Ansoft HFSS are shown in Fig. 3.7 with a good agreement. Moreover, the effective inductance of 2.5 turns, 3.5 turns, and 4.5 turns inductor are 1.842 nH, 3.587 nH, and 6.528 nH, respectively, and the peak value of Q factor for 2.5 turns, 3.5 turns, and 4.5 turns inductor are 16.16, 12.566, and 10.2, respectively. The deviation of effective inductance and Q factor between simulation and measurement are within 8%. Furthermore, the measured self resonant frequency (F_{SR}) of 2.5 turns, 3.5 turns and 4.5 turns inductor are 22.3, 14.8, and 10.5 GHz, respectively. In comparison with simulated self resonant frequency is at 21.3 GHz, 13.9 GHz, and 9.9 GHz for 2.5 turns, 3.5 turns, and 4.5 turn inductor, respectively. The F_{SR} of simulation is 1 GHz lower than measurement data. Finally, the measurement and simulation results are summarized in Table 3.2.

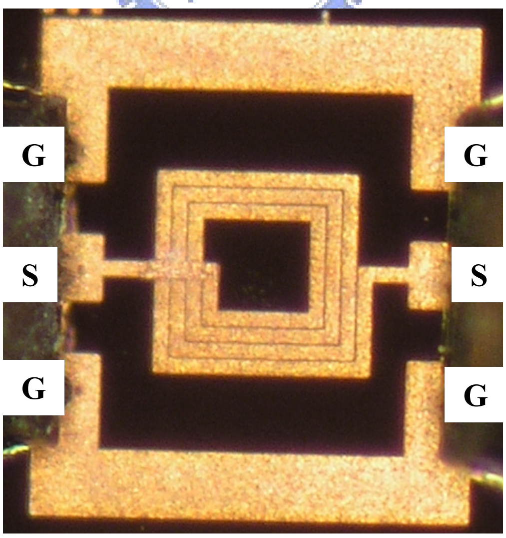

Fig. 3.6 Inductor micrograph (3.5 turns).

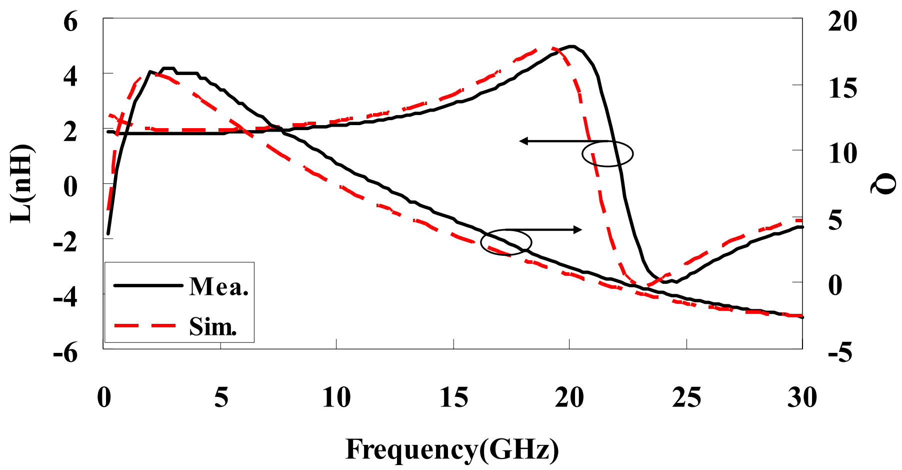

(a) 2.5 turns

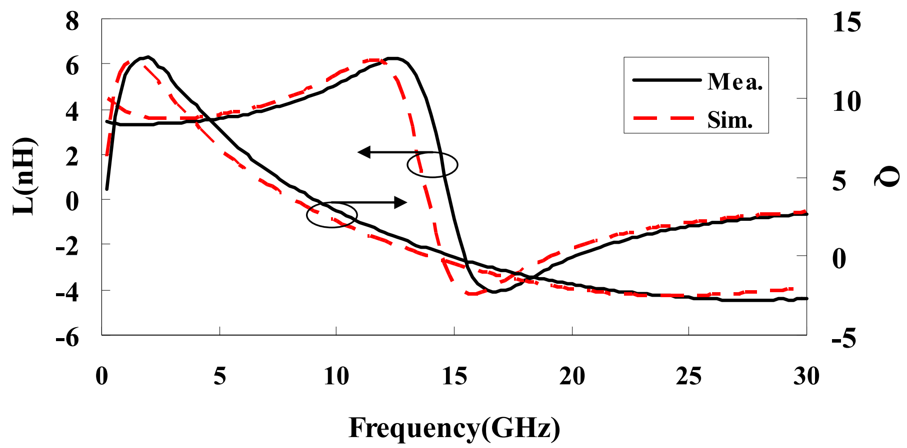

(b) 3.5 turns

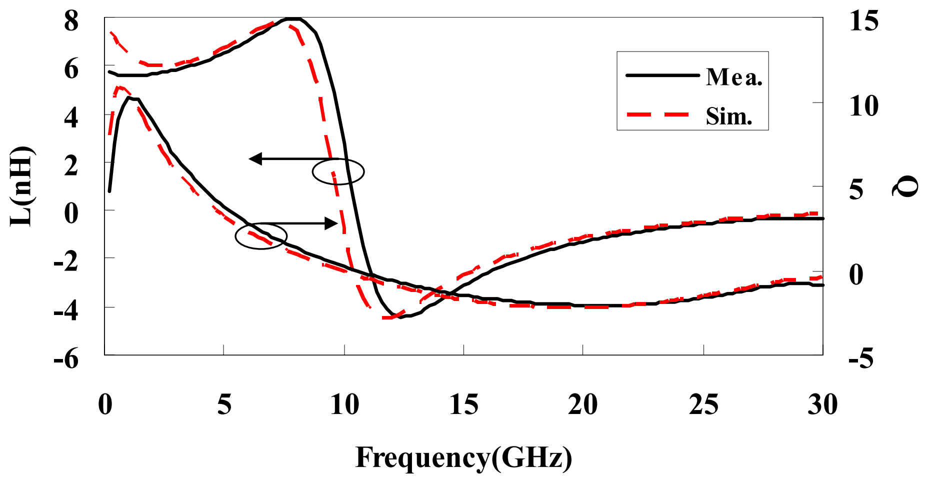

(c) 4.5 turns

Fig. 3.7 Measurement (Mea.) and simulation (Sim.) results of inductor. (a) 2.5 turns. (b) 3.5 turns. (c) 4.5 turns.

Table 3.2 Summary of inductors (measurement and simulation).

	Situation	***L (nH)@5GHz***	***Q_{peak}***	***F_{SR} (GHz)***
2.5 turns	Measurement	1.842	16.16@3GHz	22.3
	Simulation	1.974	15.648@2.4GHz	21.3
3.5 turns	Measurement	3.587	12.566@3GHz	14.8
	Simulation	3.76	12.287@1.4GHz	13.9
4.5 turns	Measurement	6.528	10.2@1GHz	10.5
	Simulation	6.723	10.817@0.6GHz	9.9

Q_{peak}: Peak Value of Q factor.

After getting the measurement data of inductor, a model is established and then used it to fit the measurement results. The traditional π model is presented in Fig. 3.8 and the meaning of the components for the equivalent circuit model is illustrated as the follows:

(1) C_p: Capacitance between adjacent metal lines.
(2) R_s: Resistance of metal line.
(3) L_s: Inductance of metal line.
(4) C_{ox1}, C_{ox2}: Capacitance between metal line and substrate.
(5) C_{sub1}, C_{sub2}: Parasitic capacitance of lossy substrate.
(6) R_{sub1}, R_{sub2}: Parasitic resistance of lossy substrate.

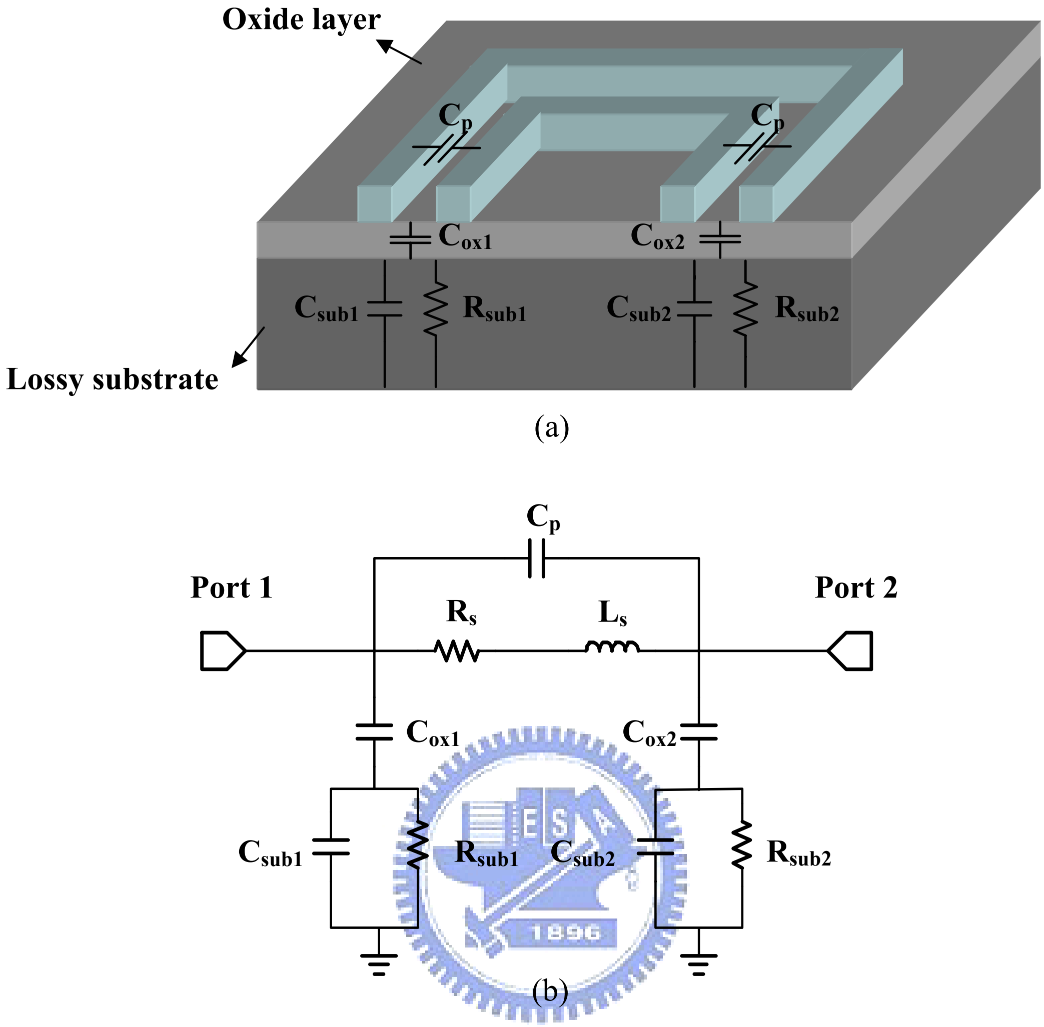

Fig. 3.8 Equivalent circuit model of the analyzed spiral inductor. (a) 3-D view. (b) Whole equivalent circuit model of the π model.

Furthermore, in order to extract these parameters of π model, a procedure is proposed to make the extraction more efficient. The procedure of parameter extraction is outlined in the following steps:

Step1. R_s and L_s: According to the equivalent model of the inductor, all the parasitic capacitances are opened as the frequency is low. Therefore, the R_s and L_s are extracted from the Y-parameters of the measurement results at the low frequency (in our case, the low frequency is 200MHz) and given, respectively by

$$\mathrm{R_s} = real\left(\frac{1}{y_{11}}\right) \quad \text{and } \mathrm{L_s} = \frac{imag(1/y_{11})}{2\pi \times frequency} \tag{3.2}$$

Where real= Real part and imag = imaginary part.

Step2. C_p: The parameter C_p is extracted from the y_{21} for the equivalent circuit model as shown in Fig. 3.9. From Fig. 3.9, the resonant frequency is given at $\frac{1}{2\pi\sqrt{L_s C_p}}$ and the C_p is read as:

$$C_p = \frac{1}{(2\pi f_{SR})L_s}, f_{SR} = self\ resonant\ frequency\ of\ y_{21} \tag{3.3}$$

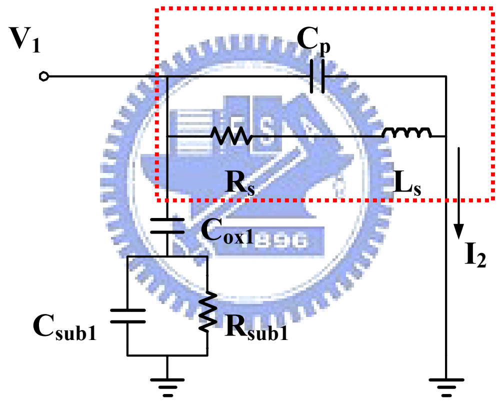

Fig. 3.9 Equivalent circuit of y_{21}.

Step3. R_{sub1}, R_{sub2}, C_{sub1}, and C_{sub2}: The parasitics of the lossy substrate start to affect the inductor as the frequency increases. Therefore, the C_{ox1} and C_{ox2} are neglected, and the equivalent circuit becomes Fig. 3.10. From Fig. 3.10, we can write:

$$Y_{in}(port\,1) = j\omega\left(C_{sub1} + C_p\right) + \frac{1}{R_{sub1}} + \frac{1}{j\omega L_s + R_s} \tag{3.4}$$

At the resonant point, we can obtain:

$$\begin{cases} C_{f_{SR}} = \dfrac{L_s}{R_s^2 + (2\pi f_{SR})^2 L_s^2} = C_{sub1} + C_p, f_{SR} = resonant\ frequency of\ Y_{in}(port1) & (3.5a) \\ R = real\left(\dfrac{1}{Y_{in}(port1)}\right) = R_{sub1}\left(\dfrac{1}{1+\dfrac{R_s C_f R_{sub1}}{L_s}}\right) & (3.5b) \end{cases}$$

We suppose the R_{sub1} is small and neglect the error term $\dfrac{R_s C_f R_{sub1}}{L_s}$ and give

$$\begin{cases} R_{sub1} \cong real\left(\dfrac{1}{Yin(port1)}\right)_{f=f_{SR}} & (3.6a) \\ C_{sub1} = \dfrac{Ls}{R_s^2 + (2\pi f_{SR})^2 L_s^2} - C_p & (3.6b) \end{cases}$$

Furthermore, we use the same method to get the R_{sub2} and C_{sub2} values as we change the Y_{in} from port 1 to port 2.

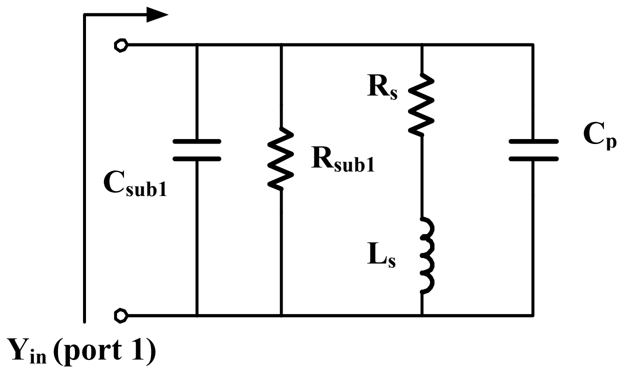

Fig. 3.10 Input admittance (Y_{in}) of port 1.

Step4. C_{ox1} **and** C_{ox2}**:** The parallel plate capacitor formula is utilized to derive the C_{ox1} and C_{ox2}. The parallel plate formula is written as:

$$C = \frac{\varepsilon A}{d}, \text{A = area of the parallel plate}$$

ε = dielectric constant that is filled between the two parallel plates

d = the distance between two parallel plates

After the initial values of the model are gained, the optimal function of the simulation tool (Agilent ADS) is utilized to obtain the final values of the equivalent circuit model.

However, the traditional π model only can fit the measurement data up to 15 GHz. Hence, in order to get a wide band frequency response (up to 30 GHz), the high frequency parasitic of the lossy substrate are taken into account and some components(R_{sub3}, C_{sub3}, L_{sub1}, L_{sub2}) are added to match the high frequency S-parameters of measurement data [7]-[9]. Therefore, the whole equivalent circuit of the wide band inductor model is shown in Fig. 3.11. As shown in Fig. 3.11, the L_{sub1} and L_{sub2} are used to model the inductive parasitic of the lossy substrate, and R_{sub3} and C_{sub3} describe another signal path from port 1 to port 2 when the frequency goes to high. Therefore, if these components are added in the traditional π model, a good agreement between modeling and measurement results can be obtained in the frequency range from 0.2 GHz to 30 GHz.

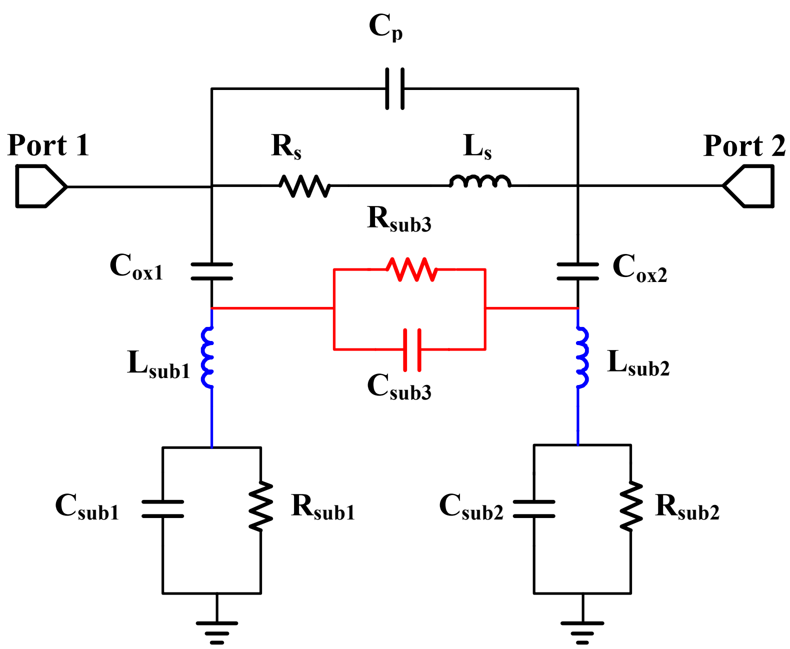

Fig. 3.11 The broad band equivalent model of spiral inductor.

Furthermore, the effective inductance and Q factor of measurement and modeling results of a spiral inductor are presented in Fig. 3.12. Form Fig. 3.12, the effective inductance of proposed inductor model is almost identical to the measurement results. And the Q factor of the model is a little large than measurement. Finally, Table 3.2 and Table 3.3 give the component list of wide band inductor model and a summary between measurement, HFSS simulation, and modeling results of the varying spiral inductors, respectively.

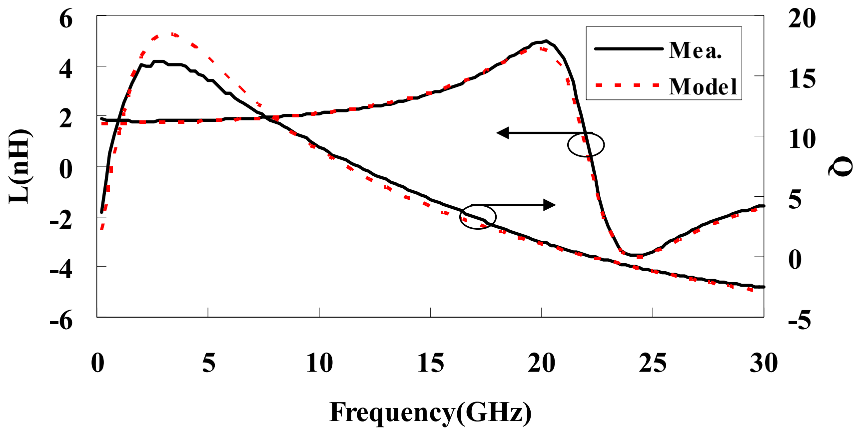

(a) 2.5 turns

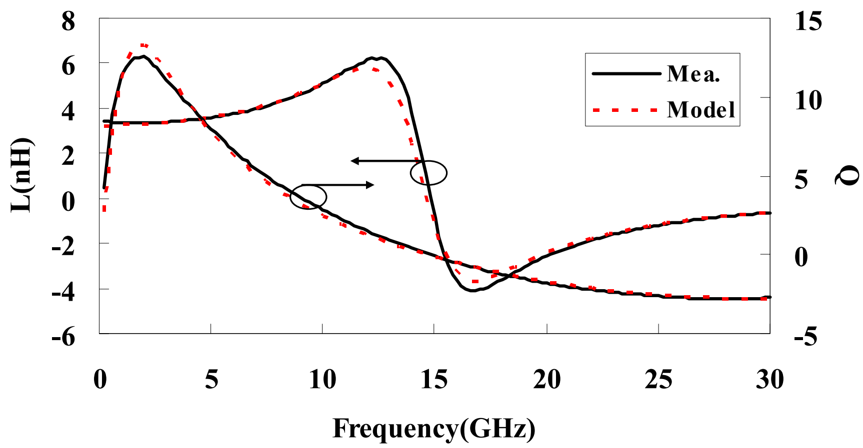

(b) 3.5 turns

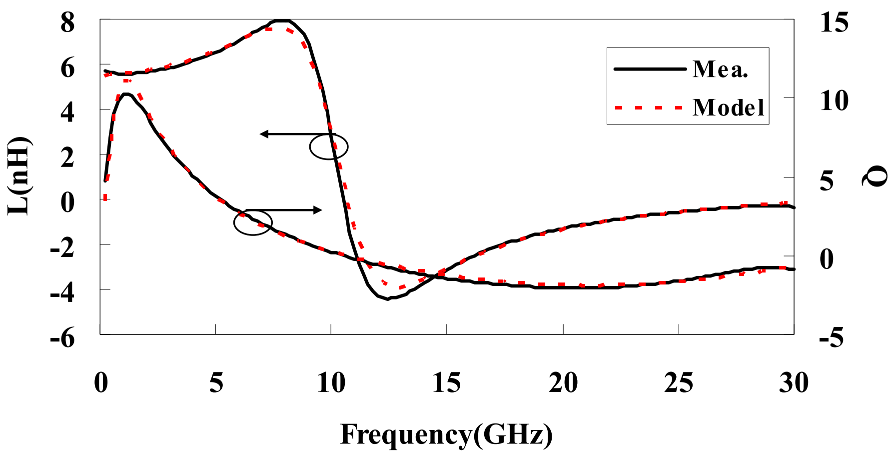

(c) 4.5 turns

Fig. 3.12 Measurement (Mea.) and modeling (Model) results of inductors. (a) 2.5 turns. (b) 3.5 turns. (c) 4.5 turn.

Table 3.3 Component list of the wide band inductor equivalent model.

Size \ *Turns*	***2.5***	***3.5***	***4.5***
$L_s(nH)$	1.73	3.232	5.422
$R_s(\Omega)$	0.977	1.486	1.965
$C_p(fF)$	8.255	12.037	13.679
$C_{ox1}(fF)$	242.824	313.848	426.241
$C_{ox2}(fF)$	307.679	394.457	495.442
$R_{sub1}(\Omega)$	1386.31	1110.61	978.768
$R_{sub2}(\Omega)$	1209.78	930.016	708.827
$C_{sub1}(fF)$	25.284	22.147	25.284
$C_{sub2}(fF)$	25.312	33.263	41.723
$R_{sub3}(\Omega)$	5218.28	4526.167	4340.981
$C_{sub3}(fF)$	1.079	1.555	1.833
$L_{sub1}(nH)$	0.246	0.631	0.979
$L_{sub2}(nH)$	0.21	0.439	0.616

Table 3.4 Summary of the spiral inductor.

	Situation	***L (nH)@5GHz***	***Q_{peak}***	***F_{SR} (GHz)***
2.5 turns	Measurement	1.842	16.16@3GHz	22.3
	Simulation	1.974	15.648@2.4GHz	21.3
	Modeling	1.810	18.427@3.2GHz	22.1
3.5 turns	Measurement	3.587	12.566@3GHz	14.8
	Simulation	3.76	12.287@1.4GHz	13.9
	Modeling	3.609	13.327@1.8GHz	14.7
4.5 turns	Measurement	6.528	10.2@1GHz	10.5
	Simulation	6.723	10.817@0.6GHz	9.9
	Modeling	6.582	11.11@1.2GHz	10.7

F_{SR}: self resonant frequency; Q_{peak}: peak value of Q factor.

3.3 Analysis of inductor coupling effects

In RF integrated circuits (RF ICs), such as LNA, mixer, and band-pass filter, the inductor is a key element for circuit designs. Unfortunately, because the substrate is lossy, the coupling effect in giga hertz frequency range is a big issue (Fig. 2.3 and Fig. 2.4). In this section, two types of inductor coupling situations are proposed (as shown in Fig.3.13) and their coupling mechanisms for different distance (d) are studied.

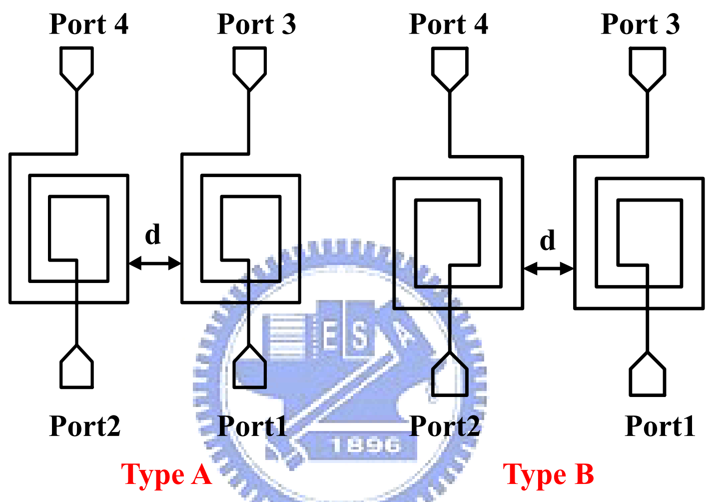

Fig. 3.13 Two type of inductor coupling situations.

3.3.1 Measurement setup and de-embedding method

The measurement instrument is the Agilent 8364B network analyzer. However, the inductor coupled pair is a four-port network, so a pair of GSGSG probes is utilized and the Agilent 8364B 4-port measurement function is used to get the 4×4 S-parameters matrix of the structure. The measurement setup is shown in Fig. 3.14.

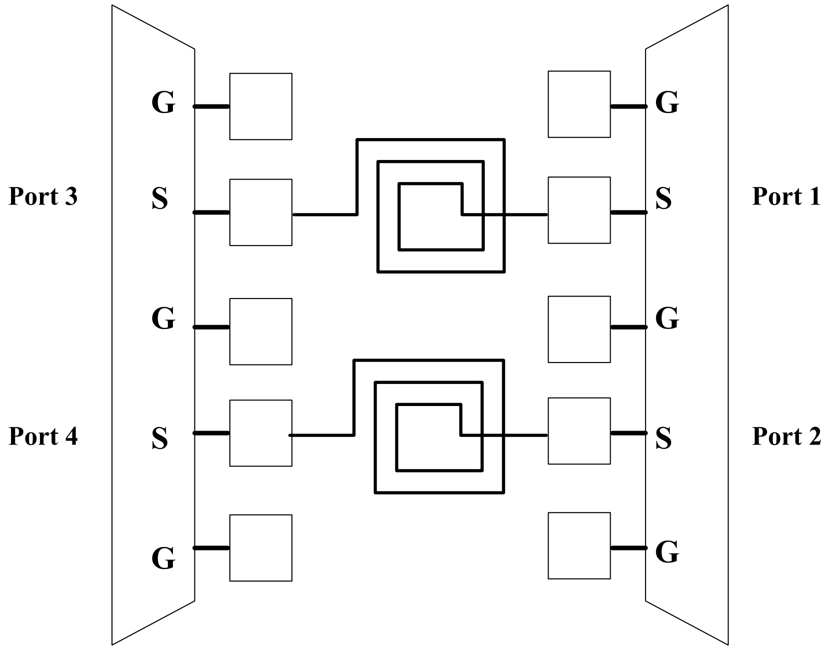

Fig. 3.14 Measurement setup of the inductor coupled pair.

As mention before, the de-embedding procedure must be done after measurement. The de-embedding procedure is almost same as stated in Section 3.2.2. The only difference is that we expand the 2×2 matrix to 4×4 matrix. The de-embedding formulas are derived as:

$$[T]_{measure} = [T]_{Z_i}[T]_{y_p}[T]_{DUT}[T]_{y_p}[T]_{Z_i}$$
$$[T]_{DUT} = [T]_{y_p}^{-1}[T]_{Z_i}^{-1}[T]_{measure}[T]_{Z_i}^{-1}[T]$$
$$then$$

$$[T]_{DUT} = \begin{bmatrix} a_1 & a_2 & a_3 & a_4 \\ b_1 & b_2 & b_3 & b_4 \\ c_1 & c_2 & c_3 & c_4 \\ d_1 & d_2 & d_3 & d_4 \end{bmatrix} \tag{3.7}$$

And the 4×4 S-parameters matrix becomes:

$$[S]_{DUT} = \begin{bmatrix} S_{11} & S_{12} & S_{13} & S_{14} \\ S_{21} & S_{22} & S_{23} & S_{24} \\ S_{31} & S_{32} & S_{33} & S_{34} \\ S_{41} & S_{42} & S_{43} & S_{44} \end{bmatrix}, \tag{3.8}$$

Where

$$S_{11} = \frac{(f_4+f_8)(k_6-k_2)+(f_2+f_6)(k_4-k_8)}{\Delta}, \tag{3.9a}$$

$$S_{12} = \frac{2(k_2k_8-k_4k_6)}{\Delta}, \tag{3.9b}$$

$$S_{13} = \frac{(f_4+f_8)(k_5k_2-k_1k_6)+(f_2+f_6)(k_1k_8-k_5k_4)+(f_1-f_5)(k_4k_6-k_2k_8)}{\Delta}, \tag{3.9c}$$

$$S_{14} = \frac{(f_2+f_6)(k_4k_7+k_3k_8)-(f_4+f_8)(k_2k_7+k_3k_6)+(f_3-f_7)(k_4k_6-k_2k_8)}{\Delta}, \tag{3.9d}$$

$$S_{21} = \frac{2(f_4f_6-f_2f_8)}{\Delta}, \tag{3.9e}$$

$$S_{22} = \frac{(k_2+k_6)(f_8-f_4)+(k_4+k_8)(f_2-f_6)}{\Delta}, \tag{3.9f}$$

$$S_{23} = \frac{(k_1-k_5)(f_2f_8-f_4f_6)-(k_2+k_6)(f_4f_5+f_1f_8)+(k_4+k_8)(f_2f_5+f_1f_6)}{\Delta}, \tag{3.9g}$$

$$S_{24} = \frac{(k_3-k_7)(f_2f_8-f_4f_6)-(k_2+k_6)(f_4f_7+f_3f_8)+(k_4+k_8)(f_2f_7+f_3f_6)}{\Delta}, \tag{3.9h}$$

$$S_{31} = \frac{-2(f_4+f_8)}{\Delta}, \tag{3.9i}$$

$$S_{32} = \frac{2(k_4+k_8)}{\Delta}, \tag{3.9j}$$

$$S_{33} = \frac{(f_4+f_8)(k_1-k_5)+(k_4+k_8)(f_5-f_1)}{\Delta}, \tag{3.9k}$$

$$S_{34} = \frac{(f_4+f_8)(k_3-k_7)+(k_4+k_8)(f_7-f_3)}{\Delta}, \tag{3.9l}$$

$$S_{41} = \frac{2(f_2+f_6)}{\Delta}, \tag{3.9m}$$

$$S_{42} = \frac{-2(k_2+k_6)}{\Delta}, \tag{3.9n}$$

$$S_{43} = \frac{(f_2+f_6)(k_5-k_1)+(k_2+k_6)(f_1-f_5)}{\Delta}, \tag{3.9o}$$

$$S_{44} = \frac{(f_2+f_6)(k_7-k_3)+(k_2+k_6)(f_3-f_7)}{\Delta}, \tag{3.9p}$$

Where $\Delta = (k_8+k_4)\ (f_6+f_2).(k_6+k_2)\ (f_4+f_8)$

$$
\text{and} \quad k_1 = a_1 - \frac{a_3}{Z_0}, \quad k_5 = c_3 - Z_0 c_1 \qquad f_1 = b_1 - \frac{b_3}{Z_0}, \quad f_5 = d_3 - Z_0 d_1
$$

$$
k_2 = a_1 + \frac{a_3}{Z_0} \quad k_6 = c_3 + Z_0 c_1, \quad \text{and} \quad f_2 = b_1 + \frac{b_3}{Z_0}, \quad f_6 = d_3 + Z_0 d_1
$$

$$
k_3 = a_2 - \frac{a_4}{Z_0}, \quad k_7 = c_4 - Z_0 c_2 \qquad f_3 = b_2 - \frac{b_4}{Z_0}, \quad f_7 = d_4 - Z_0 d_2
$$

$$
k_4 = a_2 + \frac{a_4}{Z_0}, \quad k_8 = c_4 + Z_0 c_2 \qquad f_4 = b_2 + \frac{b_4}{Z_0}, \quad f_8 = d_4 + Z_0 d_2
$$

$$
Z_0 = 50\Omega
$$

The formulas above are only the summarized results, and a complete derivation process can be referred to Appendix I.

3.3.2 Measurement results of inductor coupled pairs

The micrograph of inductor coupling pairs and measured S-parameters of type B inductor coupling pairs are presented in Fig. 3.15 and Fig. 3.16, respectively. The S_{41} of the inductor coupled pairs is taken as the amount of substrate coupling effect between two inductors. As shown in Fig. 3.16, the S_{41} is decreasing when d is increasing. And the measurement results conform to our prediction. Therefore, the inductor coupling effect will reduce if the distance between two inductors is increased. After the measurement data is obtained, the comparison between the simulation and measurement results is done and found out the measurement data reasonable or not. And the simulation tool is Ansoft HFSS, too. From Fig. 3.16, the measured S_{41} is lower then simulation and the maximum deviation of S_{41} is less than 1 dB. Therefore, the good agreement between measurement and simulation is obtained. Furthermore, to inspect the S_{41} value of 2.5 turns inductor coupled pairs and 3.5 turns inductor coupled pairs, it can be observed the S_{41} is slightly dependent on the frequency.

Moreover, the differences of S_{41} for different types of inductor coupled pairs are also observed. As presented in Fig. 3.17, the S_{14} of type A is smaller then type B. The phenomenon is because that the inductor coupled pairs of type B has the longer metal lines in opposition to each other. As a result, the metal line induces the larger coupling effect between two inductors. Furthermore, the magnetic flux of type B is larger than that of type A; it is also a reason that the S_{41} value of type B is larger than that of type A.

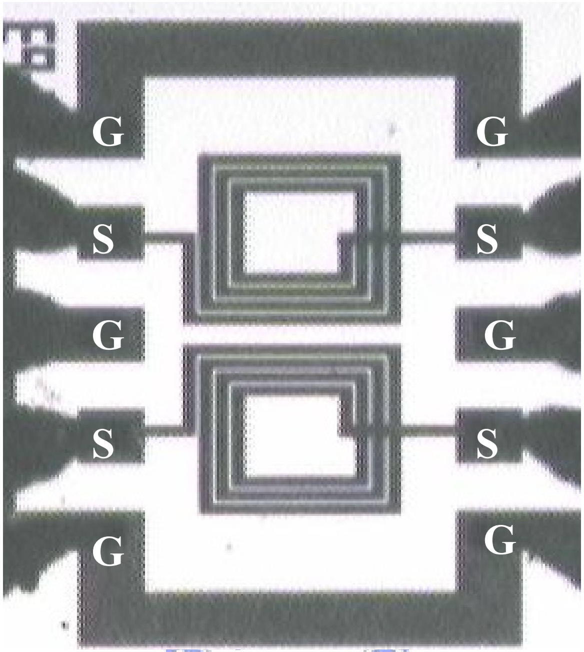

Fig.3.15 Micrograph of inductor the coupling pair (3.5 turns typeB with d=30um).

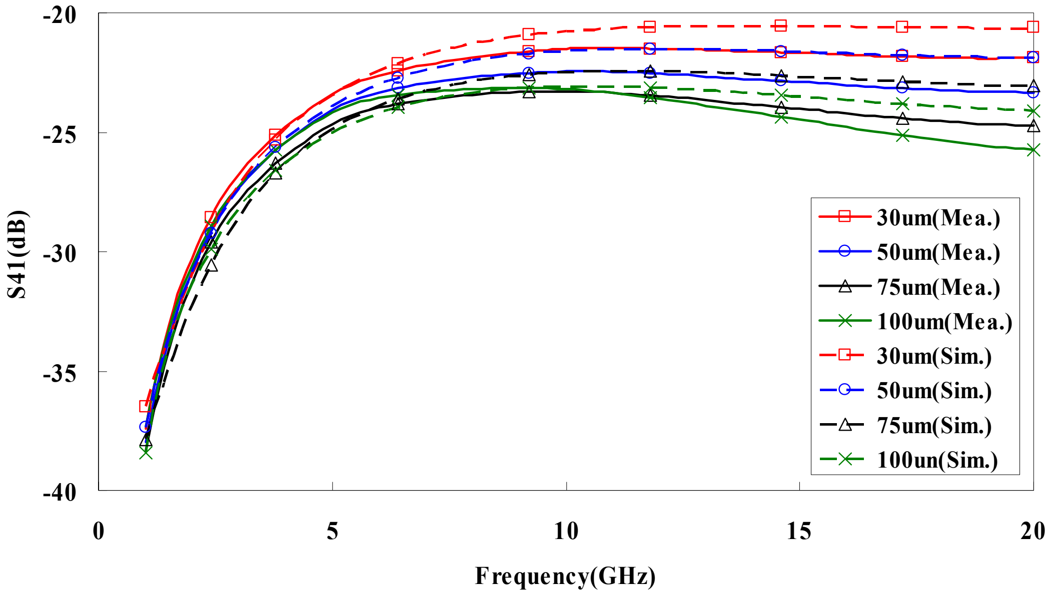

(a)

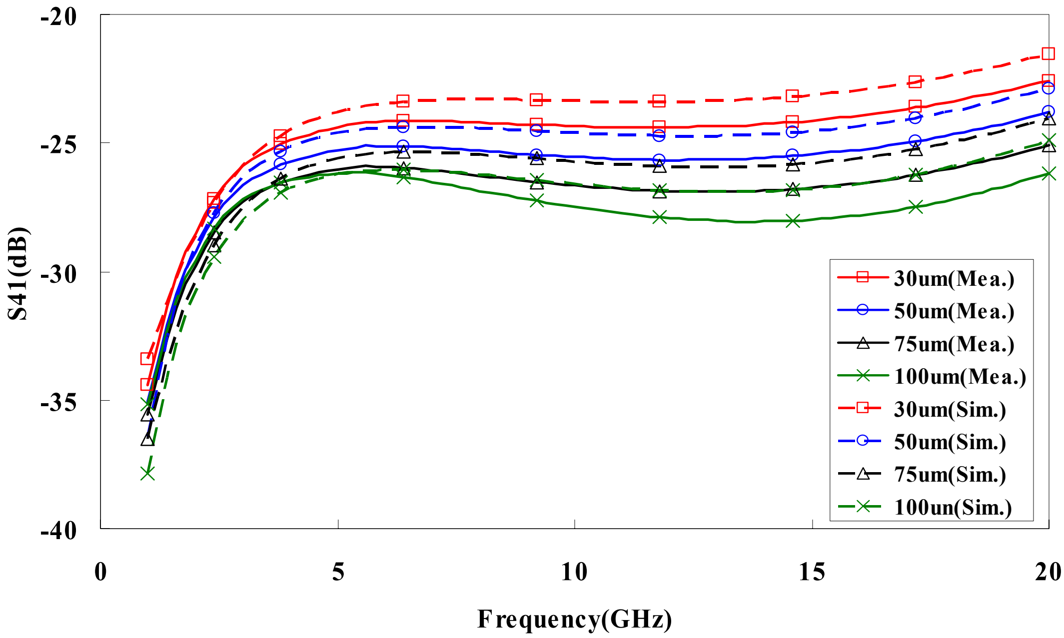

(b)

Fig. 3.16 Measurement (Mea.) and simulation (Sim.) result of the inductor coupled pairs for the varying separate distance. (a) 2.5 turns, type B. (b) 3.5 turns, type B.

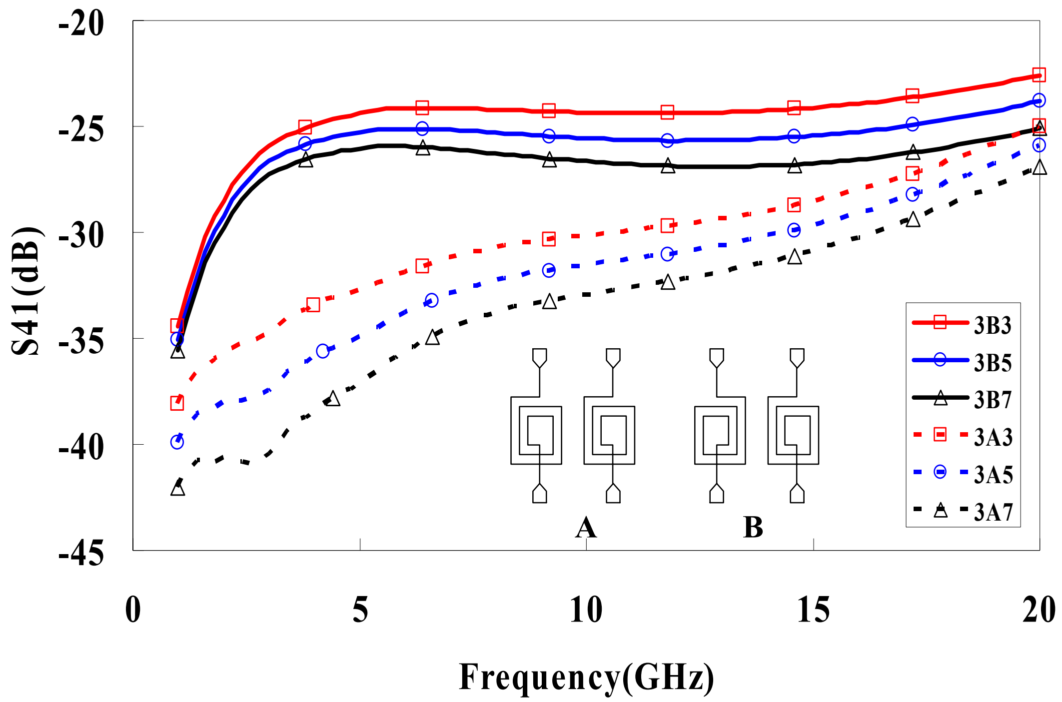

Notes:

(1) 3.5 turns type A
d=30um: 3A3
d=50um: 3A5
d=75um: 3A7

(2) 3.5 turns type B
d=30um: 3A3
d=50um: 3A5
d=75um: 3A7

Fig.3.17 Comparison of different types for 3.5 turns inductor coupled pairs.

3.3.3 Discussion about the inaccuracy between measurement and simulation results

To compare the measurement and simulation results, the trend of simulation curve is similar to that of measurement, but the overall S_{41} values are about 1 dB larger than measurement results for different distances. Hence, we attempt to find the 1dB variation between simulation and measurement results. We suppose that the source of variation comes from the process we used. First, the oxide thickness is confirmed, and the oxide thickness is almost equal with 2.1 um after measurement. Second, the effective dielectric constant of the oxide is varied from 3.9 to 3, and the variation of S_{41} is within 0.1 dB. As a result, the effective dielectric constant is not the main fact that can cause the S_{41} deviation. And the last, the conductivity of the wafer is checked. The conductivity=4 (Siemens/m) is used in the simulation. But when the conductivity is changed from 4 to 5 (Siemens/m), the simulation curve is more similar to the measurement one. Fig. 3.18 and Fig. 3.19 present the improved simulation results and compare them with measurement curve for the 2.5 turns and 3.5 turns inductor coupled pairs, respectively. Therefore, the variation of conductivity of the wafer is the main factor that causes the variation between measurement and simulation results.

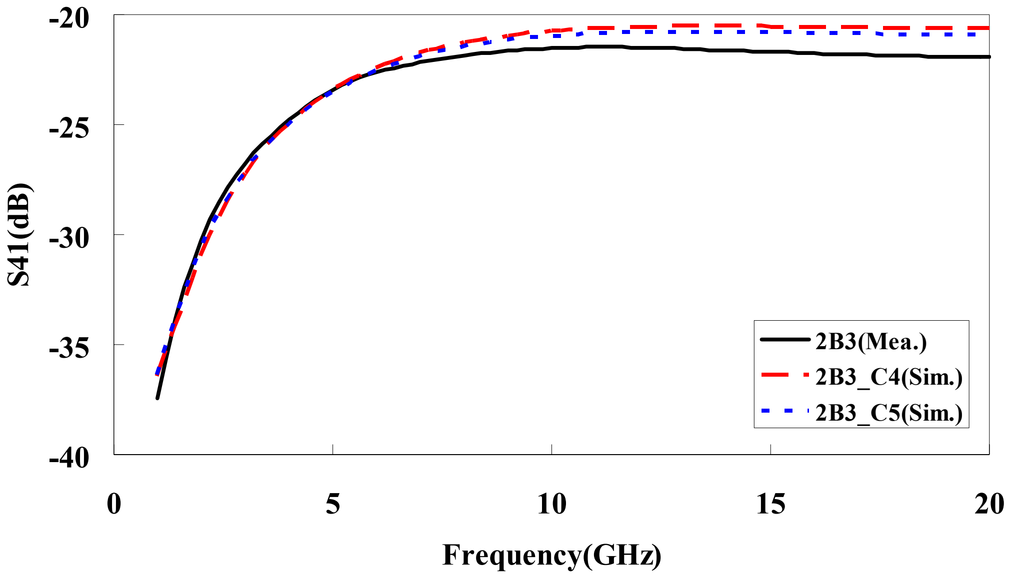

(a)

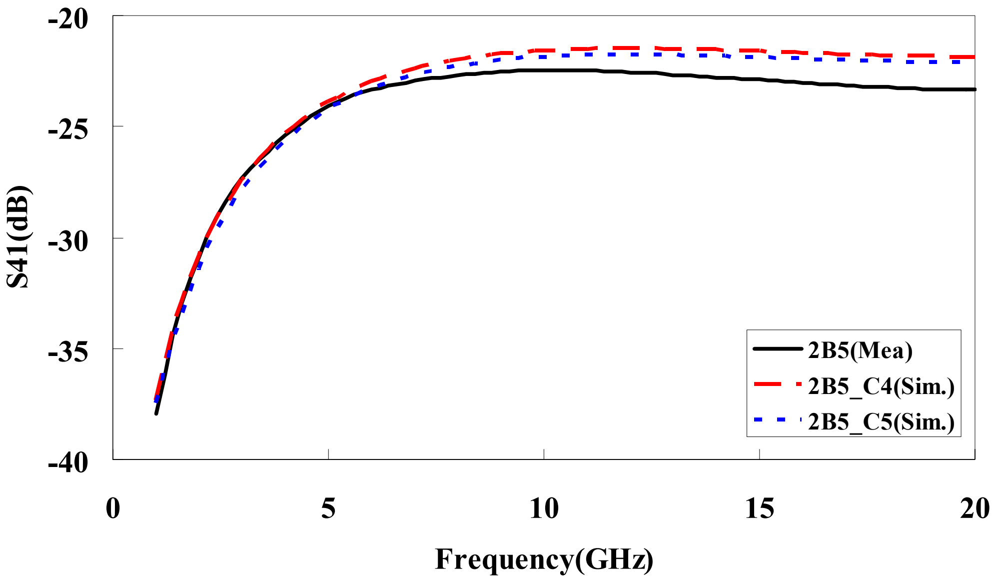

(b)

Notes:

(1) 2.5 turns, type B

d=30 um, conductivity of wafer=4 (Seimens/m): 2B3_C4

d=30 um, conductivity of wafer=5 (Seimens/m): 2B3_C5

d=50 um, conductivity of wafer=4 (Seimens/m): 2B5_C4

d=50 um, conductivity of wafer=5 (Seimens/m): 2B5_C5

Fig. 3.18 Improved simulation (Sim.) and measurement (Mea.) result for the 2.5 turns type B inductor coupled pairs. (a) d=30um. (b) d=50um.

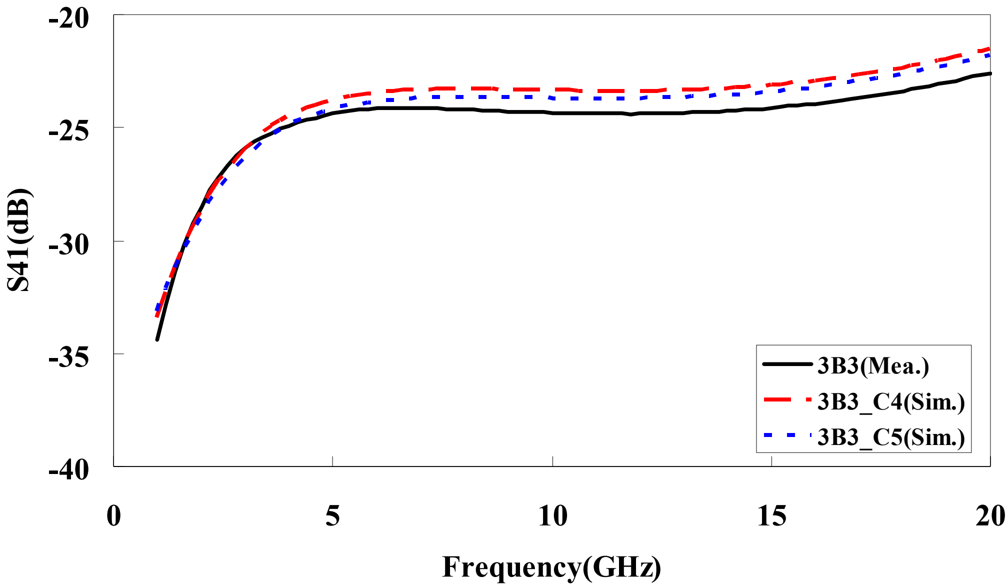

(a)

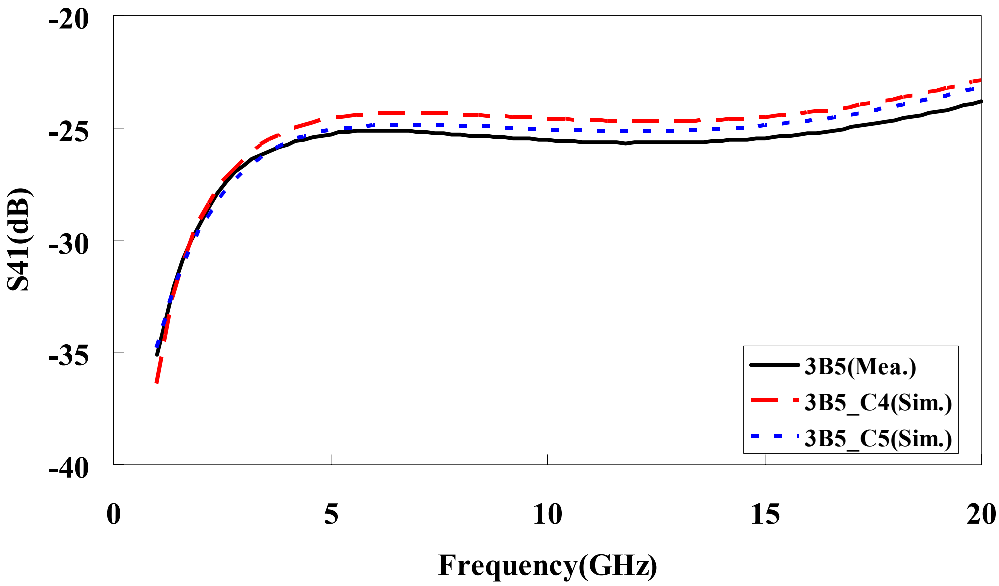

(b)

Notes:

(1) 3.5 turns, type B

d=30 um, couductivity of wafer=4 (Seimens/m): 3B3_C4
d=30 um, couductivity of wafer=5 (Seimens/m): 3B3_C5
d=50 um, couductivity of wafer=4 (Seimens/m): 3B5_C4
d=50 um, couductivity of wafer=5 (Seimens/m): 3B5_C5

Fig.3.19 Improved simulation (Sim.) and measurement (Mea.) results for the 3.5 turns type B inductor coupled pairs. (a) d=30um. (b) d=50um.

3.3.4 Modeling of inductor coupled pairs

Having acquired the measurement data of inductor coupled pairs; a model is constructed to represent their noise coupling behavior. First, a RC parallel network (R_{sub4}, R_{sub5}, C_{sub4}, and C_{sub5}) is established to describe the electrical noise coupling effect in the lossy substrate. Second, the coupling coefficient (k) is exploited and it can express the magnetic coupling effect between two inductors. Finally, these two parts are combined with the wide band inductor model and the whole equivalent circuit model is presented in Fig. 3.20.

Fig. 3.21 shows the modeling results of 2.5 turns type B inductor coupling pair, and the meaning of 2B3, 2B5, and 2B7 are corresponding to d=30um, d=50um, d=75um, respectively. As observed in Fig. 3.21, the difference between modeling and measurement results is only within 0.3 dB. Moreover, the proposed model can represent the curve of coupling effect from 1 GHz~15 GHz and the component values of the coupling circuit is listed in Table 3.4.

Moreover, the scaling formulas of the inductor coupled pairs are also derived from the extracted parameters (R_{sub4}, R_{sub5}, C_{sub4}, C_{sub5}, and k). And the formulas are shown as the follows:

$$R_{sub4}=-0.129d2+57.778d+3630.7\ (\Omega) \quad (3.10a)$$

$$R_{sub5}=-0.3949d2+89.275d+2311.5\ (\Omega) \quad (3.10b)$$

$$C_{sub4}=-0.0624d+7.352\ (fF) \quad (3.10c)$$

$$C_{sub5}=-0.0601d+6.9979\ (fF) \quad (3.10d)$$

$$k=-0.0007d+0.2025 \quad (3.10e)$$

d=um

Therefore, the circuit designers can refer to these formulas and understand the coupling effect for any distance.

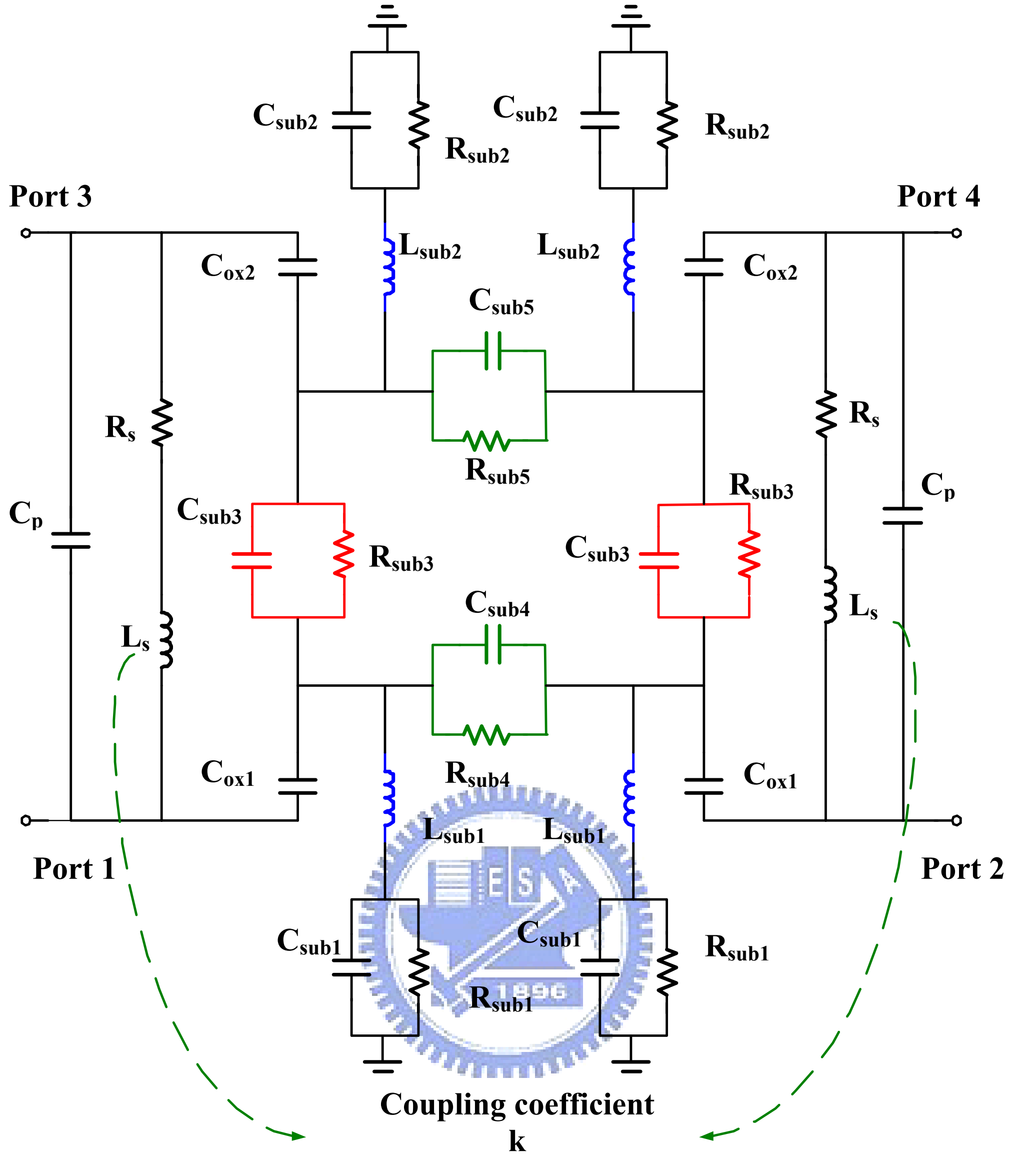

(1) The definition of ports is the same with Fig.3.12
(2) $C_{sub4}||R_{sub4}$: The electrical noise coupling between Port 1and Port 2
(3) $C_{sub5}||R_{sub5}$: The electrical noise coupling between Port 3and Port 4
(4) Coupling coefficient (k): Magnetic coupling between two inductors

Fig. 3.20 Equivalent circuit of the inductor coupled pairs.

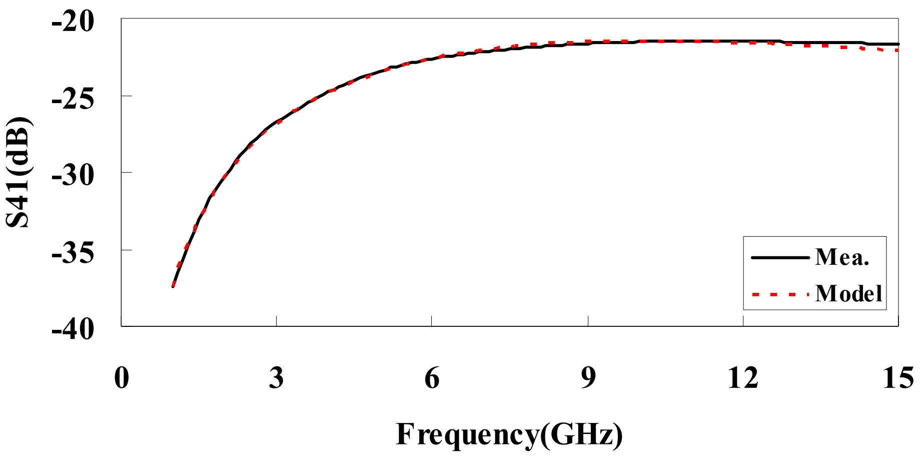
-20
-25
-30
-35
-40
S41(dB)
Mea.
Model
0
3
6
9
12
15
Frequency(GHz)

(a)

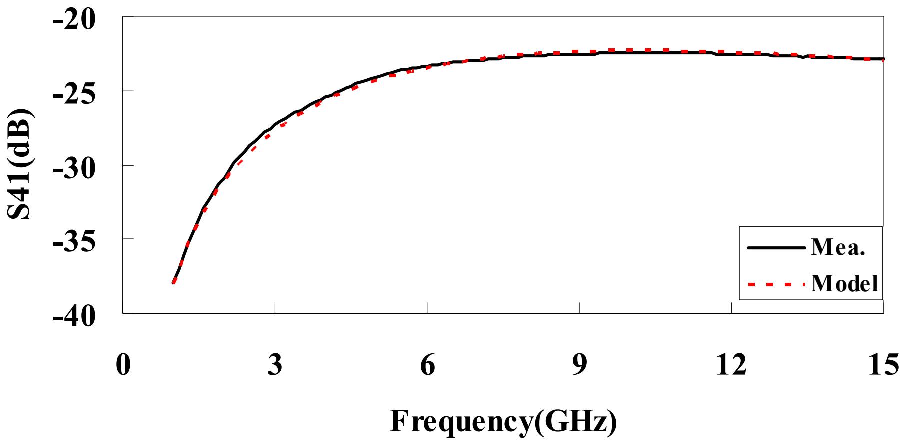
-20
-25
-30
-35
-40
S41(dB)
Mea.
Model
0
3
6
9
12
15
Frequency(GHz)

(b)

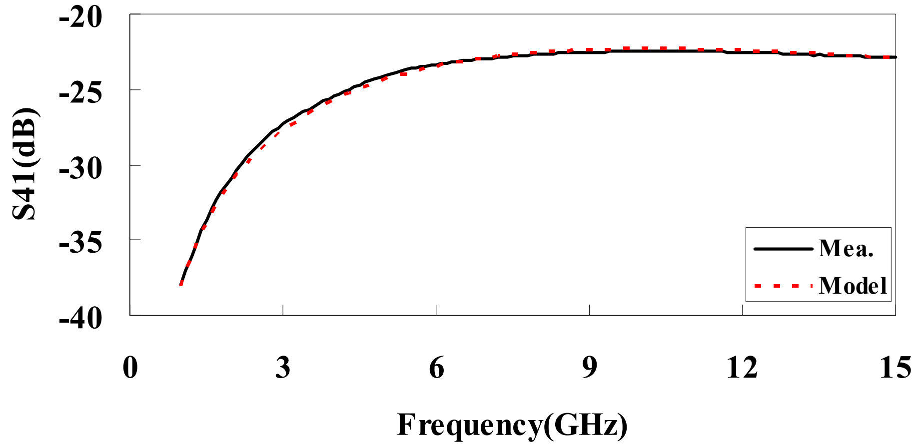

(c)

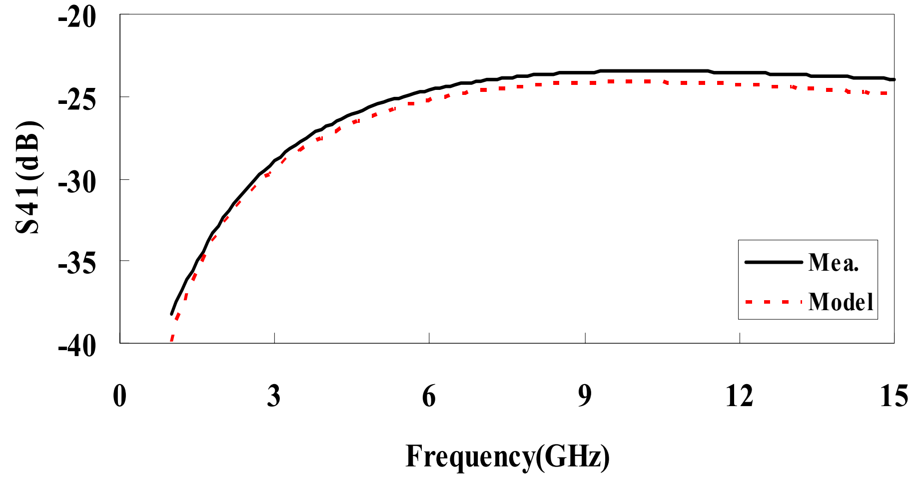

(d)

Note:

(1) 2.5 turns type B
d=30um: 2B3
d=50um: 2B5
d=75um: 2B7
d=100um: 2B1

Fig. 3.21 Measurement (Mea.) and Modeling (Model) results. (a) 2B3. (b) 2B5. (c) 2B7. (d) 2B1.

Table 3.5 Component list of the equivalent circuit of 2.5 turns type B inductor coupled pairs.

d(um) / Component	**30**	**50**	**75**	**100**
$R_{sub4}(\Omega)$	5281.7	6111.07	7312.56	8090.65
$R_{sub5}(\Omega)$	4609.75	5849.66	6730..65	7307.25
$C_{sub4}(fF)$	5.34	4.492	2.549	1.12
$C_{sub5}(fF)$	5.165	4.113	2.225	1.09
k	0.1818	0.1643	0.1493	0.13

3.4 Comparison with other works

When the measurement and modeling results is done, we try to compare the results with the publication data. First, from [10] and [11], the measurement method is the two-port measurement case with the other terminals being open or floating (as depicted in Fig.3.22). On the contrary, our measurement data are the four-port S-parameters matrix with all ports at the 50 Ω terminations. Those measurement data are more useful for RF circuit designers to apply them for the post-simulation procedure before the chip tape out.

Moreover, in the part of proposed equivalent circuit of inductor coupled pairs, the frequency range is up to 15 GHz with the deviation of 0.3 dB. According to [11], its frequency range of equivalent model is only about 10 GHz and the deviation between measurement and model is larger than 1 dB. As a result, the proposed model can explore the coupling effect of inductor coupled pairs more accurately.

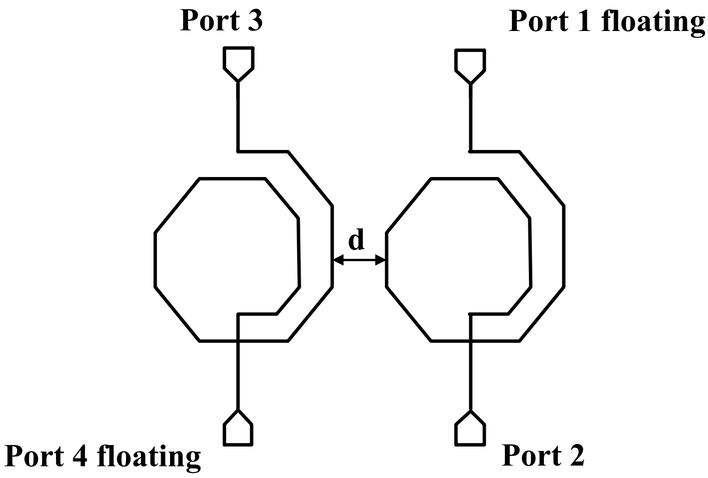

Fig. 3.22 Sketch of the inductor coupling pair in [10].

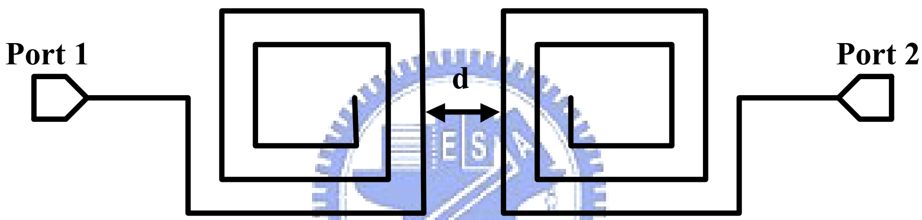

Fig. 3.23 Sketch of the inductor coupling pair in [11].

Table 3.6 Comparison with other papers.

	This work	***Ref.[10]***	***Ref.[11]***
Process	Home-made process on 21-23Ω-cm P-type substrate	0.25um, 5-level metal, CMOS process on 10Ω-cm p-type substrate	0.25um, 4-level metal, logic-CMOS process on 10Ω-cm P-type substrate
Measurement	Full four ports	Two ports (other ports floating)	Two ports (other ports floating)
Modeling	1 GHz -15 GHz	N/A	1 GHz -10 GHz
Error (Sim. and Mea.)	About 1dB	N/A	N/A
Error (Mea. and Model.)	0.3 dB	About 1dB	N/A

N/A: Not available.

3.5 Summary and contributions

In Section 3.2, the wide band model for spiral inductor is proposed and the improved model represents the good agreement from 0.2 GHz to 30 GHz. Moreover, the coupling effect of two inductors is discussed in Section 3.3. The simulation method can predict the coupling effect precisely with the error of 1 dB between the simulation and measurement results. Utilizing the simulation method can understand the coupling effect between inductors. Thus, the circuit designers can use the method to avoid the unwanted coupling effect during the circuit design procedure.

Besides, the equivalent model of inductor coupled pairs is also proposed. The equivalent circuit model shows the good performance in the range of 1 GHz -15 GHz. This is also the useful information for RF circuit designers.

Finally, the contributions and differentiations from the other papers are summarized as the follows:

(1) A full four ports simulation, de-embedding, and measurement procedure for inductor coupling is done. The papers ([10] and [11]) are only the two-port measurement results with other ports being floating. Moreover, a good agreement between the simulation and measurement data is obtained in our study.

(2) The equivalent circuit of 2.5 turns type B inductor coupled pairs is established in the frequency range of 1 GHz to 15 GHz. Besides, the equivalent circuit takes the electrical and magnetic parasitics into account at the same time.

CHAPTER 4

Substrate Noise Coupling Effect in TSMC 0.18um CMOS Process

In this chapter, the substrate coupling effects in TSMC 0.18um CMOS process are studied. First, the testkey is designed to investigate the substrate coupling effect between two P^+(or N^+) contacts in N-well (or P-well). Furthermore, the distance between two contacts is changed and it can find the substrate coupling effect for different distance. Therefore, the behavior of noise propagating in the lossy silicon substrate can be realized.

4.1 Testkey design

In the testkey, several types of test patterns are designed to study the substrate coupling effect in different well (P-well and N-well). As presented in Fig. 4.1, two P^+ (or N^+) contacts are formed with area=15×15 um^2 in P-well (or N-well), and then vary the distance (d) between two contacts to observe the amount (S_{21} of the two-port network) of substrate coupling effect. Thus, the propagation of substrate noise in the lossy substrate can be observed. Moreover, a summary of the testkey is listed in Table 4.1.

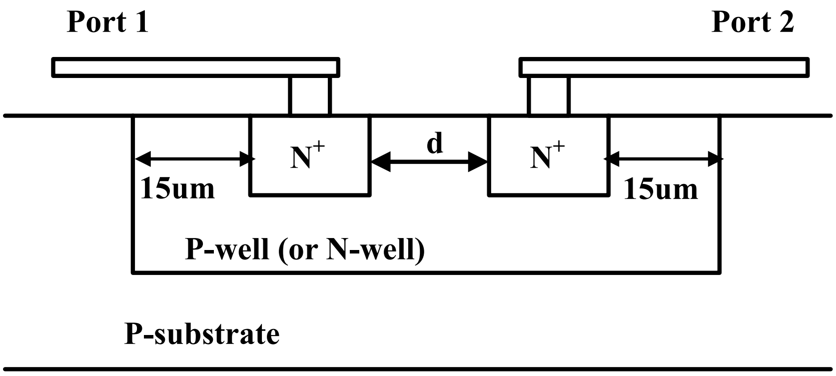

(a)

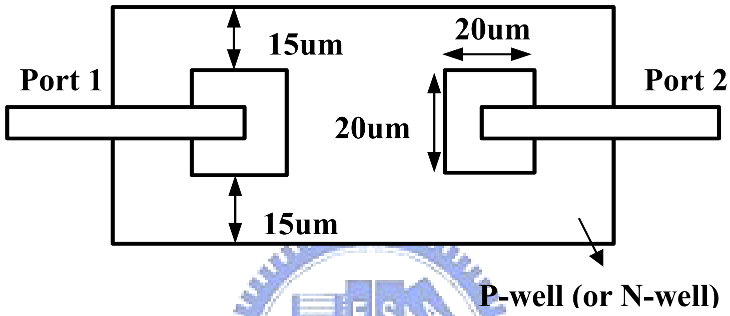

(b)

Fig. 4.1 Structure of the test pattern. (a) Cross-section view. (b) Top view.

Table 4.1 Specification of the testkey.

	P-well	***N-well***
d(um)	N^+~N^+	P^+~P^+
50	●	●
75	●	●
100	●	●
125	●	N/A

N/A: Not available.

4.2 Measurement results

The micrograph of the testkey is shown in Fig. 4.2. The row 1 and row 4 are the test patterns. The measurement setup is presented as Fig. 4.3 and the Agilent 8364B network analyzer and a pair of GSG probes with pitch size 100 um are used during measurement. Therefore, The S_{21} measurement results of the two-port network as the quantity of substrate noise in substrate, the substrate noise as shown in Fig. 4.4 is reducing when the distance(d) becomes longer. And the relationship between quantity of noise coupling and distance seems to be linear. Moreover, the measurement data show the quantity of substrate noise coupling is almost independent of frequency. Therefore, the measurement results imply that substrate noise coupling effect is almost resistive in the lossy substrate.

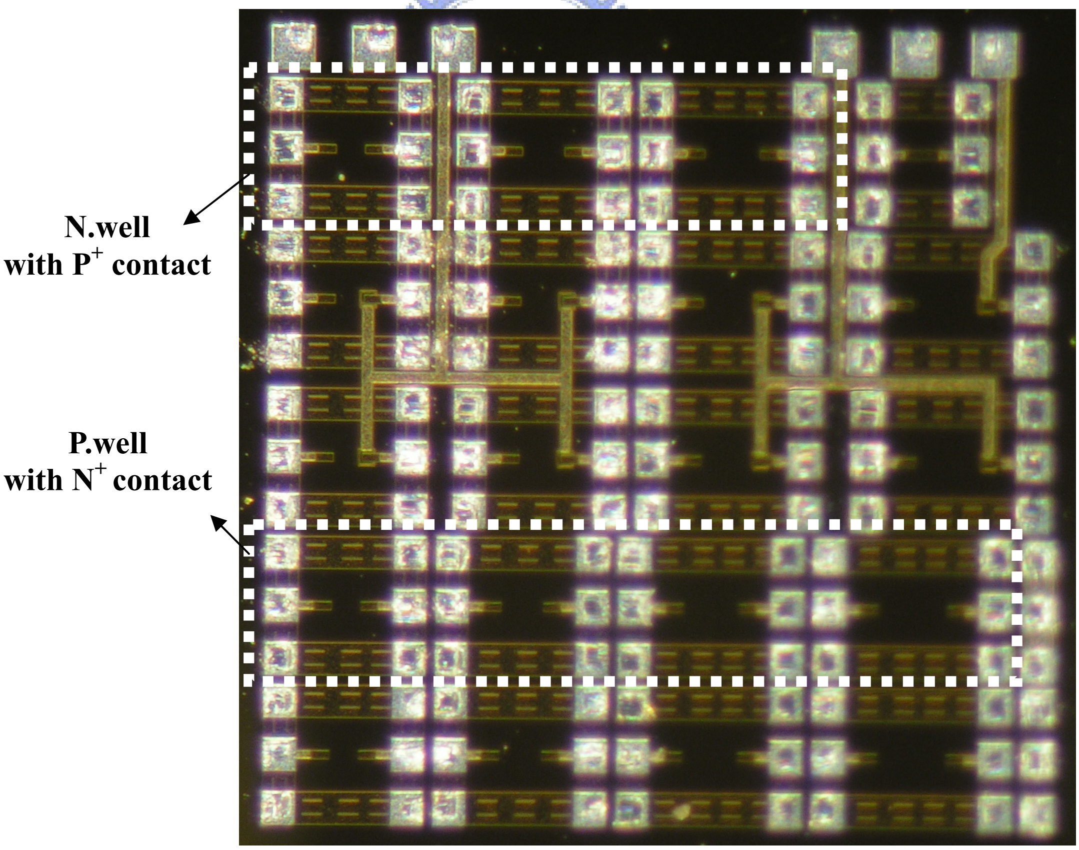

Fig. 4.2 Micrograph of the testkey.

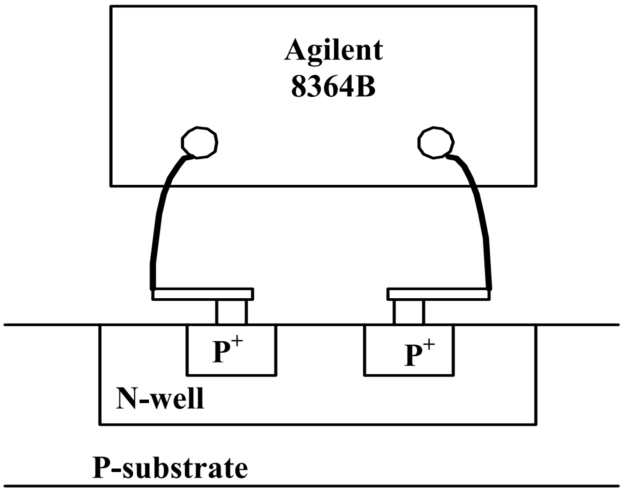

(a)

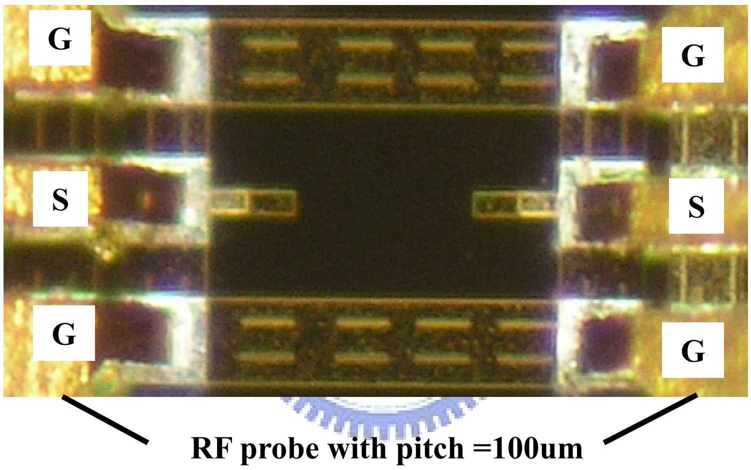

(b)

Fig. 4.3 Measurement setup. (a) Connect to network analyzer. (b) Test pattern (P-well with N+ contact and d=125 um) with probing.

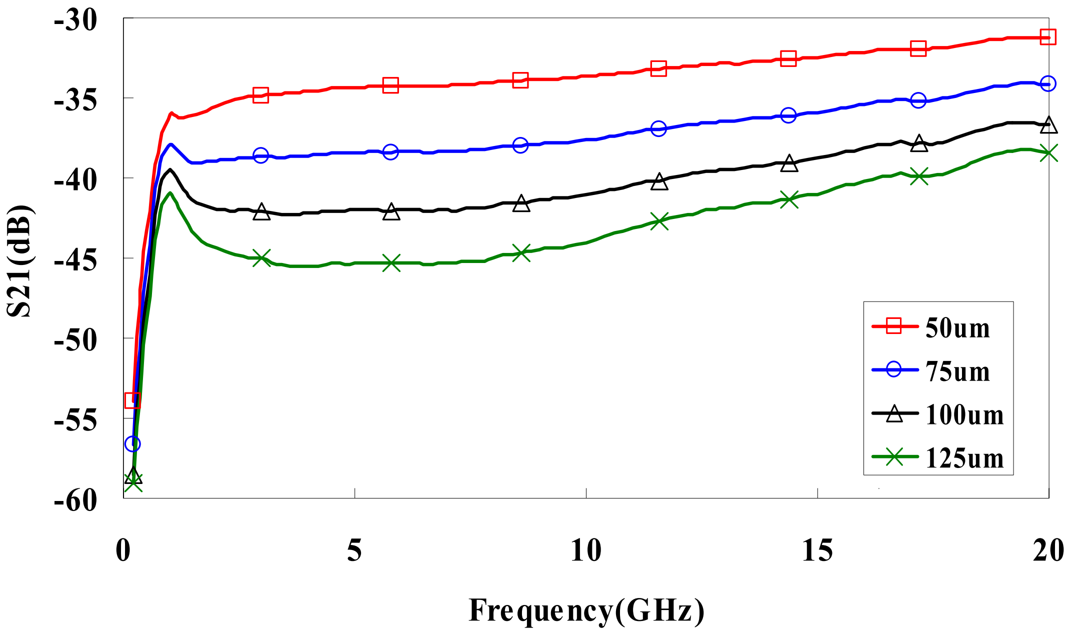

(a)

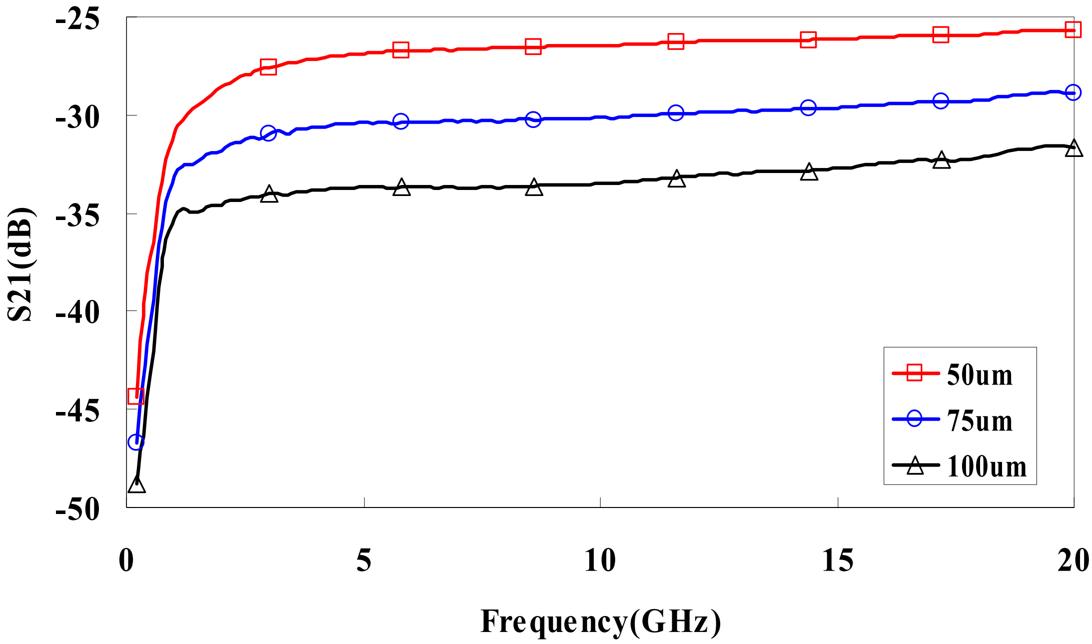

(b)

Fig. 4.4 Measurement results. (a) P-well with N^+ contacts. (b) N-well with P^+ contacts.

CHAPTER 5

Conclusion and Future Works

5.1 Conclusion

In the thesis, the coupling effect of two adjacent inductors is presented first. Moreover, a wide band model of single spiral inductor is also built up. The inductor model can fit the effective inductor and Q factor from 0.2 GHz to 30 GHz in correlation with the measurement. In the part of inductor coupled pairs, the measurement data indicate the coupling effect between two inductors is less than -20dB. Moreover, we also realize the coupling effect of inductor coupled pairs is slightly dependent on the separate distance. As a result, to increase the distance and suppress the noise coupling effect between two inductors is not an efficient way.

From the measurement results of type A and type B, the quantity of S_{41} are not equal. The results give a hint that the coupling effect is related to the layout style of inductors. And the proper layout style can reduce the coupling effect of adjacent inductors. After the measurement results of inductor coupled pairs are obtained, an equivalent circuit model is established to illustrate the coupling effect. The proposed model can precisely predict the coupling behavior from 1 GHz to 15 GHz.

The substrate noise coupling phenomenon in TSMC 0.18um CMOS process is discussed, too. In this part, the substrate coupling effect of two P^+ (or N^+) contacts in N-well (P-well) is analyzed. According to the measurement result, we find the substrate coupling effect is not strongly dependent on the frequency.

Above all, the measurement and modeling results give the important information for RF circuit designers. The designers can refer to the information and decrease the parasitic effect of inductors. Therefore, a more efficient RF circuit design procedure can be realized.

5.2 Future works

As the model established in Section 3.3.4, the model of inductor coupling can explore the coupling behavior from 1 GHz to 15GHz. The frequency range is not wide enough for RF circuit designers. As a result, how to increase the frequency range is the most important thing to do.

Moreover, the inductor coupled pairs used in RF circuit designs is not only the type we propose. There are many different layout styles of inductor coupled pairs. Hence, to find their coupling mechanisms and sum up those results is the significant task, too

Finally, we investigate the substrate noise coupling effect in TSMC 0.18um CMOS process. The situation we investigate is passive like. The coupling effect of active device, such as MOSFET and BJT, is not discussed in the thesis. Therefore, as the operation frequency goes to high (up to 60 GHz), the study about the substrate noise coupling effect of active device is an urgent issue for RF circuit designs.

REFERENCES

[1] D. K. Su, M. J. Loinaz, S. Masui, and B. A. Wooley, "Experimental Result and Modeling Techniques for Substrate Noise in Mixed.signal Integrated Circuits," *IEEE J. Solid-State Circuits*, vol. 28, pp. 420-430, Apr. 1993.

[2] T. Gabara, "Reduced Ground Bounce and Improved Latch up Suppression through Substrate Condition," *IEEE J. Solid-State Circuits*, vol. 23, pp. 1224-1232, Oct. 1988.

[3] R. B. Merrill, W. M. Young, and K. Brehmer, "Effect of Substrate Material in Mixed Analog/Digital Integrated Circuits," in P*roc. IEEE Int. Electron Devices Meeting*, pp. 433-436, San Francisco, CA, Dec. 1994.

[4] J. W. Lin, "*An Optimum Design of the Micromachined RF Inductor*" Master's thesis, Dept. of Electronics Engineering and Inst. of Electronics, NCTU, Taiwan, 2004.

[5] Troels Emil Kolding, "On-Wafer Calibration Techniques for giga-hertz CMOS Measurement," *in Proc. ICMTS*, pp.105.110, March 1999.

[6] D. M. Polar, *Microwave Engineering*, Third edition, John Wiley & Sons, Inc., 2005.

[7] C. J. Chao, S. C. Wong, C. H. Kao, M. J. Chen, L. Y. Leu, and K. Y. Chiu, "Characterization and Modeling of On-Chip Spiral Inductors for Si-RFICs," *IEEE Trans. on semiconductor manufacturing*, pp. 19-29, Feb. 2002.

[8] T. S. Horng, J. K. Jau, C. H. Huang, and T. Y. Han, "Synthesis of a Super Broadband Model for On-Chip Spiral Inductors," *IEEE RFIC Symposium*, pp.453-456, June 2004.

[9] Joonho Gil, and Hyungcheol Shin, "A Simple Wide-Band On-Chip Inductor Model for Silicon-Based RF ICs," *IEEE Trans. Microwave Theory and Techniques,*

vol. 51, pp. 2023-2028, Step. 2003.

[10] C. J. Chao, S. C. Wong, C. J. Hsu, M. J. Chen, and L. Y. Leu, "Characterization and Modeling of On-Chip Inductor Substrate Coupling Effect," *IEEE RFIC Symposium*, pp. 311-314, June 2002.

[11] A. O. Adan, M. Fukumi, K. Higashi, T. Suyma, M. Miyamoto, and M. Hayshi, "Electromagnetic Coupling Effects in RFCMOS Circuits," *IEEE RFIC Symposium*, pp. 293-296, June 2002.

[12] M. Werthen, I. Wolff, R. Keller,and W. Bischof, "Investigation of MMIC Inductor Coupling Effect," *IEEE MTT-S International*, vol.3, pp. 1793.1796, June 1997.

Appendix I

Four-Port Transformation

Because considering the model for the pad parasitic as Z_i and y_p, the equivalent circuit of our DUT (with pad parasitic) is shown in Fig. 1. Therefore, we derive the transmission matrix of the pad parasitic and use the de-embedding procedure to obtain the correct measurement result of our four-port network.

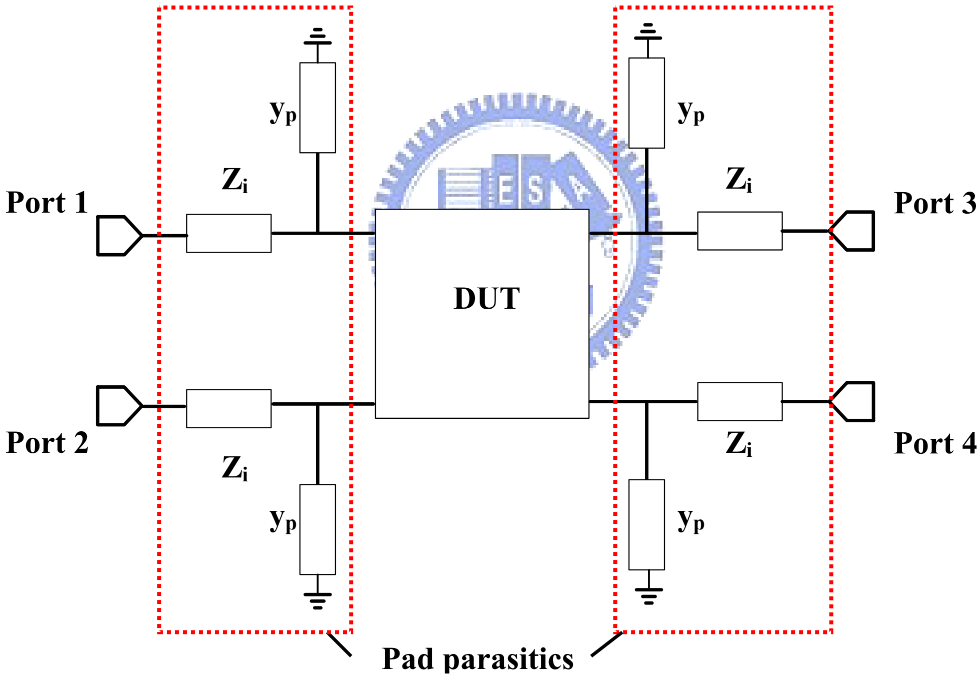

Fig. 1 The four-port network with pad parasitics.

A. Transmission matrix of Z circuit

The Z circuit is presented in Fig. 2. From the definition of transmission matrix, we can derive that:

$$\begin{bmatrix} V_1 \\ V_2 \\ I_1 \\ I_2 \end{bmatrix} = \begin{bmatrix} a_1 & a_2 & a_3 & a_4 \\ b_1 & b_2 & b_3 & b_4 \\ c_1 & c_2 & c_3 & c_4 \\ d_1 & d_2 & d_3 & d_4 \end{bmatrix} \begin{bmatrix} V_3 \\ V_4 \\ I_3 \\ I_4 \end{bmatrix}, where \begin{bmatrix} a_1 & a_2 & a_3 & a_4 \\ b_1 & b_2 & b_3 & b_4 \\ c_1 & c_2 & c_3 & c_4 \\ d_1 & d_2 & d_3 & d_4 \end{bmatrix} = \begin{bmatrix} 1 & 0 & Z_1 & 0 \\ 0 & 1 & 0 & Z_2 \\ 0 & 0 & 1 & 0 \\ 0 & 0 & 0 & 1 \end{bmatrix} = [T]_{Z\ circuit}$$

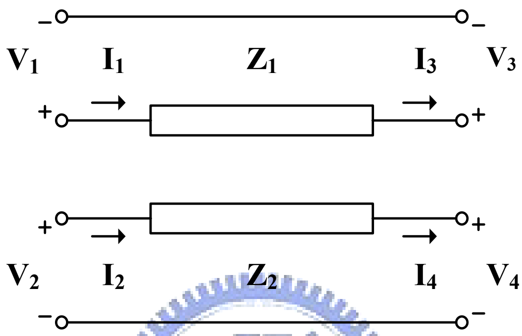

Fig. 2 Z circuit.

B. Transmission matrix of Y circuit

The concept to obtain Y circuit as depicted in Fig. 3 is the same as Part A and we can derive:

$$\begin{bmatrix} V_1 \\ V_2 \\ I_1 \\ I_2 \end{bmatrix} = \begin{bmatrix} a_1 & a_2 & a_3 & a_4 \\ b_1 & b_2 & b_3 & b_4 \\ c_1 & c_2 & c_3 & c_4 \\ d_1 & d_2 & d_3 & d_4 \end{bmatrix} \begin{bmatrix} V_3 \\ V_4 \\ I_3 \\ I_4 \end{bmatrix}, where \begin{bmatrix} a_1 & a_2 & a_3 & a_4 \\ b_1 & b_2 & b_3 & b_4 \\ c_1 & c_2 & c_3 & c_4 \\ d_1 & d_2 & d_3 & d_4 \end{bmatrix} = \begin{bmatrix} 1 & 0 & 0 & 0 \\ 0 & 1 & 0 & 0 \\ Y_1 & 0 & 1 & 0 \\ 0 & Y_2 & 0 & 1 \end{bmatrix} = [T]_{Y\ circuit}$$

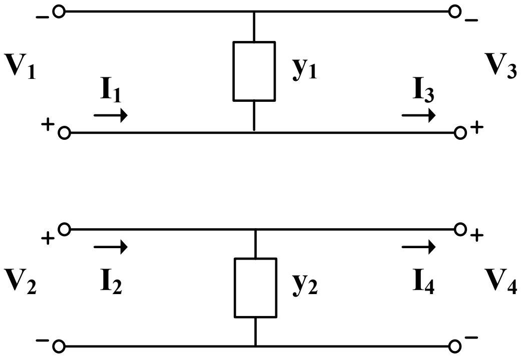

Fig. 3 Y circuits.

C. Transform between four-port S-parameters and transmission matrix

(1) S-parameters to transmission matrix

$$\begin{bmatrix} V_1^- \\ V_2^- \\ V_3^- \\ V_4^- \end{bmatrix} \begin{bmatrix} S_{11} & S_{12} & S_{13} & S_{14} \\ S_{21} & S_{22} & S_{23} & S_{24} \\ S_{31} & S_{32} & S_{33} & S_{34} \\ S_{41} & S_{42} & S_{43} & S_{44} \end{bmatrix} = \begin{bmatrix} V_1^+ \\ V_2^+ \\ V_3^+ \\ V_4^+ \end{bmatrix} \xrightarrow{\textit{transfer}} \begin{bmatrix} V_1 \\ V_2 \\ I_1 \\ I_2 \end{bmatrix} \begin{bmatrix} a_1 & a_2 & a_3 & a_4 \\ b_1 & b_2 & b_3 & b_4 \\ c_1 & c_2 & c_3 & c_4 \\ d_1 & d_2 & d_3 & d_4 \end{bmatrix} = \begin{bmatrix} V_3 \\ V_4 \\ I_3 \\ I_4 \end{bmatrix}$$

for

$$\begin{cases} V_1 = V_1^+ + V_1^- \\ V_2 = V_2^+ + V_2^- \\ V_3 = V_3^+ + V_3^- \\ V_4 = V_4^+ + V_4^- \end{cases} \textit{and} \begin{cases} I_1 = \dfrac{V_1^+ - V_1^-}{Z_0}, I_3 = \dfrac{V_3^- - V_3^+}{Z_0} \\ I_2 = \dfrac{V_2^+ - V_2^-}{Z_0}, I_4 = \dfrac{V_4^- - V_4^+}{Z_0} \end{cases}$$

we can obtain

$$V_1^+ + V_1^- = (S_{11}+1)V_1^+ + S_{12}V_2^+ + S_{13}V_3^+ + S_{14}V_4^+$$
$$V_2^+ + V_2^- = S_{21}V_1^+ + (S_{22}+1)V_2^+ + S_{23}V_3^+ + S_{24}V_4^+$$
$$V_3^+ + V_3^- = S_{31}V_1^+ + S_{32}V_2^+ + (S_{33}+1)V_3^+ + S_{34}V_4^+$$
$$V_4^+ + V_4^- = S_{41}V_1^+ + S_{42}V_2^+ + S_{43}V_3^+ + (S_{44}+1)V_4^+$$

and

$$\frac{V_1^+ - V_1^-}{Z_0} = \frac{1-S_{11}}{Z_0}V_1^+ - \frac{S_{12}}{Z_0}V_2^+ - \frac{S_{13}}{Z_0}V_3^+ - \frac{S_{14}}{Z_0}V_4^+$$
$$\frac{V_2^+ - V_2^-}{Z_0} = \frac{-S_{21}}{Z_0}V_1^+ + \frac{(1-S_{22})}{Z_0}V_2^+ - \frac{S_{23}}{Z_0}V_3^+ - \frac{S_{24}}{Z_0}V_4^+$$
$$\frac{V_3^- - V_3^+}{Z_0} = \frac{S_{31}}{Z_0}V_1^+ + \frac{S_{32}}{Z_0}V_2^+ + \frac{(S_{33}-1)}{Z_0}V_3^+ + \frac{S_{34}}{Z_0}V_4^+$$
$$\frac{V_4^- - V_4^+}{Z_0} = \frac{S_{41}}{Z_0}V_1^+ + \frac{S_{42}}{Z_0}V_2^+ + \frac{S_{43}}{Z_0}V_3^+ + \frac{(S_{44}-1)}{Z_0}V_4^+$$

So,

$$\begin{bmatrix} V_1 \\ V_2 \\ I_1 \\ I_2 \end{bmatrix} = \begin{bmatrix} 1+S_{11} & S_{12} & S_{13} & S_{14} \\ S_{21} & 1+S_{22} & S_{23} & S_{24} \\ \dfrac{1-S_{11}}{Z_0} & \dfrac{-S_{12}}{Z_0} & \dfrac{-S_{13}}{Z_0} & \dfrac{-S_{14}}{Z_0} S_{34} \\ \dfrac{-S_{21}}{Z_0} & \dfrac{1-S_{22}}{Z_0} & \dfrac{-S_{23}}{Z_0} & \dfrac{-S_{24}}{Z_0} \end{bmatrix} \begin{bmatrix} S_{31} & S_{32} & 1+S_{33} & S_{34} \\ S_{41} & S_{42} & S_{43} & S_{44} \\ \dfrac{S_{31}}{Z_0} & \dfrac{S_{32}}{Z_0} & \dfrac{S_{33}-1}{Z_0} & \dfrac{S_{34}}{Z_0} \\ \dfrac{S_{41}}{Z_0} & \dfrac{S_{42}}{Z_0} & \dfrac{S_{43}}{Z_0} & \dfrac{S_{44}-1}{Z_0} \end{bmatrix}^{-1} \begin{bmatrix} V_3 \\ V_4 \\ I_3 \\ I_4 \end{bmatrix}$$

$$[T]=\begin{bmatrix} a_1 & a_2 & a_3 & a_4 \\ b_1 & b_2 & b_3 & b_4 \\ c_1 & c_2 & c_3 & c_4 \\ d_1 & d_2 & d_3 & d_4 \end{bmatrix}=\begin{bmatrix} 1+S_{11} & S_{12} & S_{13} & S_{14} \\ S_{21} & 1+S_{22} & S_{23} & S_{24} \\ \frac{1-S_{11}}{Z_0} & \frac{-S_{12}}{Z_0} & \frac{-S_{13}}{Z_0} & \frac{-S_{14}}{Z_0} S_{34} \\ \frac{-S_{21}}{Z_0} & \frac{1-S_{22}}{Z_0} & \frac{-S_{23}}{Z_0} & \frac{-S_{24}}{Z_0} \end{bmatrix}\begin{bmatrix} S_{31} & S_{32} & 1+S_{33} & S_{34} \\ S_{41} & S_{42} & S_{43} & S_{44} \\ \frac{S_{31}}{Z_0} & \frac{S_{32}}{Z_0} & \frac{S_{33}-1}{Z_0} & \frac{S_{34}}{Z_0} \\ \frac{S_{41}}{Z_0} & \frac{S_{42}}{Z_0} & \frac{S_{43}}{Z_0} & \frac{S_{44}-1}{Z_0} \end{bmatrix}^{-1}$$

Hence,

$$a_1=\frac{1}{2}S_{13}+\frac{S_{12}[S_{41}(S_{33}-1)-S_{31}S_{43}]+(1+S_{11})[S_{42}(S_{33}-1)+S_{32}S_{43}]}{\eta}$$

$$a_2=\frac{1}{2}S_{14}+\frac{S_{12}[S_{31}(1-S_{44})+S_{34}S_{41}]+(1+S_{11})[S_{32}(S_{44}-1)-S_{34}S_{42}]}{\eta}$$

$$a_3=Z_0(-\frac{1}{2}S_{13}+\frac{S_{12}[-S_{41}(1+S_{33})+S_{31}S_{43}]+(1+S_{11})[S_{42}(1+S_{33})-S_{32}S_{43}]}{\eta})$$

$$a_4=Z_0(-\frac{1}{2}S_{14}+\frac{S_{12}[S_{31}(1+S_{44})-S_{34}S_{41}]+(1+S_{11})[-S_{32}(1+S_{44})+S_{34}S_{42}]}{\eta})$$

and

$$b_1=\frac{1}{2}S_{23}+\frac{S_{21}[S_{42}(1-S_{33})+S_{32}S_{43}]+(1+S_{22})[S_{41}(S_{33}-1)-S_{31}S_{43}]}{\eta}$$

$$b_2=\frac{1}{2}S_{24}+\frac{S_{21}[S_{32}(S_{44}-1)-S_{34}S_{42}]+(1+S_{22})[S_{31}(1-S_{44})+S_{34}S_{41}]}{\eta}$$

$$b_3=Z_0(-\frac{1}{2}S_{23}+\frac{S_{21}[S_{42}(1+S_{33})-S_{32}S_{43}]+(1+S_{22})[-S_{41}(1+S_{33})+S_{31}S_{43}]}{\eta})$$

$$b_4=Z_0(-\frac{1}{2}S_{24}+\frac{S_{21}[-S_{32}(1+S_{44})+S_{34}S_{42}]+(1+S_{22})[S_{31}(1+S_{44})-S_{34}S_{41}]}{\eta})$$

and

$$c_1=\frac{1}{Z_0}(-\frac{1}{2}S_{13}+\frac{S_{12}[S_{41}(1-S_{33})+S_{31}S_{43}]+(1-S_{11})[S_{42}(1-S_{33})+S_{32}S_{43}]}{\eta})$$

$$c_2=\frac{1}{Z_0}(-\frac{1}{2}S_{14}+\frac{-S_{12}[S_{31}(1-S_{44})+S_{34}S_{41}]+(1-S_{11})[S_{32}(S_{44}-1)-S_{34}S_{42}]}{\eta})$$

$$c_3=\frac{1}{2}S_{13}+\frac{S_{12}[S_{41}(1+S_{33})-S_{34}S_{41}]+(1-S_{11})[S_{42}(1+S_{33})-S_{32}S_{43}]}{\eta}$$

$$c_4=\frac{1}{2}S_{14}+\frac{-S_{12}[S_{31}(1+S_{44})-S_{34}S_{41}]+(1-S_{11})[-S_{32}(1+S_{44})+S_{34}S_{42}]}{\eta}$$

$$d_1 = \frac{1}{Z_0}\left(-\frac{1}{2}S_{23} + \frac{-S_{21}[S_{42}(1-S_{33}) + S_{32}S_{43}] + (1-S_{22})[-S_{41}(1-S_{33}) - S_{31}S_{43}]}{\eta}\right)$$

$$d_2 = \frac{1}{Z_0}\left(-\frac{1}{2}S_{24} + \frac{S_{21}[S_{32}(1-S_{44}) + S_{34}S_{42}] + (1-S_{22})[S_{31}(1-S_{44}) + S_{34}S_{41}]}{\eta}\right)$$

$$d_3 = \frac{1}{2}S_{23} + \frac{-S_{21}[S_{42}(1+S_{33}) - S_{32}S_{43}] + (1-S_{22})[-S_{41}(1+S_{33}) + S_{31}S_{43}]}{\eta}$$

$$d_4 = \frac{1}{2}S_{24} + \frac{S_{21}[S_{32}(1+S_{44}) - S_{34}S_{42}] + (1-S_{22})[S_{31}(1+S_{44}) - S_{34}S_{41}]}{\eta}$$

η *is defined as* :

$$\Rightarrow \eta = 2(S_{31}S_{42} - S_{32}S_{41})$$

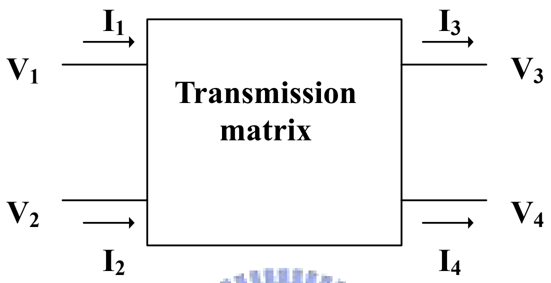

Fig. 4 Four-port transmission matrix.

(2) Transmission matrix to S-parameters

$$\begin{bmatrix} V_1 \\ V_2 \\ I_1 \\ I_2 \end{bmatrix} = \begin{bmatrix} a_1 & a_2 & a_3 & a_4 \\ b_1 & b_2 & b_3 & b_4 \\ c_1 & c_2 & c_3 & c_4 \\ d_1 & d_2 & d_3 & d_4 \end{bmatrix} \begin{bmatrix} V_3 \\ V_4 \\ I_3 \\ I_4 \end{bmatrix}, where \begin{cases} V_1 = V_1^+ + V_1^- & V_3 = V_3^+ + V_3^- \\ I_1 = \dfrac{V_1^+ - V_1^-}{Z_0} & I_3 = \dfrac{1}{Z_0}(V_3^- - V_3^+) \\ V_2 = V_2^+ + V_2^- & V_4 = V_4^+ + V_4^- \\ I_2 = \dfrac{V_2^+ - V_2^-}{Z_0} & I_4 = \dfrac{1}{Z_0}(V_4^- - V_4^+) \end{cases}$$

Hence,

$$\Rightarrow \begin{cases} V_1^+ + V_1^- = a_1(V_3^+ + V_3^-) + a_2(V_4^+ + V_4^-) + a_3\dfrac{1}{Z_0}(V_3^- - V_3^+) + a_4\dfrac{1}{Z_0}(V_4^- - V_4^+) \\ V_2^+ + V_2^- = b_1(V_3^+ + V_3^-) + b_2(V_4^+ + V_4^-) + b_3\dfrac{1}{Z_0}(V_3^- - V_3^+) + b_4\dfrac{1}{Z_0}(V_4^- - V_4^+) \\ V_1^+ + V_1^- = Z_0c_1(V_3^+ + V_3^-) + Z_0c_2(V_4^+ + V_4^-) + c_3(V_3^- - V_3^+) + c_4(V_4^- - V_4^+) \\ V_1^+ + V_1^- = Z_0d_1(V_3^+ + V_3^-) + Z_0d_2(V_4^+ + V_4^-) + d_3(V_3^- - V_3^+) + d_4(V_4^- - V_4^+) \end{cases}$$

then

$$\begin{cases} V_1^- = -V_1^+ + (a_1 - \dfrac{a_3}{Z_0})V_3^+ + (a_1 + \dfrac{a_3}{Z_0})V_3^- + (a_2 - \dfrac{a_4}{Z_0})V_4^+ + (a_2 + \dfrac{a_4}{Z_0})V_4^- \\ V_2^- = -V_2^+ + (b_1 - \dfrac{b_3}{Z_0})V_3^+ + (b_1 + \dfrac{b_3}{Z_0})V_3^- + (b_2 - \dfrac{b_4}{Z_0})V_4^+ + (b_2 + \dfrac{b_4}{Z_0})V_4^- \\ V_1^- = V_1^+ + (c_3 - Z_0c_1)V_3^+ - (c_3 + Z_0c_1)V_3^- + (c_4 - Z_0c_2)V_4^+ - (c_4 + Z_0c_2)V_4^- \\ V_2^- = V_2^+ + (d_3 - Z_0d_1)V_3^+ - (d_3 + Z_0d_1)V_3^- + (d_4 - Z_0d_2)V_4^+ - (d_4 + Z_0d_2)V_4^- \end{cases}$$

let $k_1 = a_1 - \dfrac{a_3}{Z_0}, \quad k_5 = c_3 - Z_0c_1 \qquad f_1 = b_1 - \dfrac{b_3}{Z_0}, \quad f_5 = d_3 - Z_0d_1$

$k_2 = a_1 + \dfrac{a_3}{Z_0} \quad k_6 = c_3 + Z_0c_1$, and $f_2 = b_1 + \dfrac{b_3}{Z_0}, \quad f_6 = d_3 + Z_0d_1$

$k_3 = a_2 - \dfrac{a_4}{Z_0}, \quad k_7 = c_4 - Z_0c_2 \qquad f_3 = b_2 - \dfrac{b_4}{Z_0}, \quad f_7 = d_4 - Z_0d_2$

$k_4 = a_2 + \dfrac{a_4}{Z_0}, \quad k_8 = c_4 + Z_0c_2 \qquad f_4 = b_2 + \dfrac{b_4}{Z_0}, \quad f_8 = d_4 + Z_0d_2$

we can obtain

$$\begin{cases} V_1^- = -V_1^+ + k_1V_3^+ + k_2V_3^- + k_3V_4^+ + k_4V_4^- \\ V_1^- = V_1^+ + k_5V_3^+ - k_6V_3^- + k_7V_4^+ - k_8V_4^- \\ V_2^- = -V_2^+ + f_1V_3^+ + f_2V_3^- + f_3V_4^+ + f_4V_4^- \\ V_2^- = V_2^+ + f_5V_3^+ - f_6V_3^- + f_7V_4^+ - f_8V_4^- \end{cases} \Rightarrow \begin{cases} V_1^- - k_2V_3^- - k_4V_4^- = -V_1^+ + k_1V_3^+ + k_3V_4^+ \\ V_1^- + k_6V_3^- + k_8V_4^- = V_1^+ + k_5V_3^+ + k_7V_4^+ \\ V_2^- - f_2V_3^- - f_4V_4^- = -V_2^+ + f_1V_3^+ + f_3V_4^+ \\ V_2^- + f_6V_3^- + f_8V_4^- = V_2^+ + f_5V_3^+ + f_7V_4^+ \end{cases}$$

So,

$$\begin{bmatrix} 1 & 0 & -k_2 & -k_4 \\ 1 & 0 & k_6 & k_8 \\ 0 & 1 & -f_2 & -f_4 \\ 0 & 1 & f_6 & f_8 \end{bmatrix} \begin{bmatrix} V_1^- \\ V_2^- \\ V_3^- \\ V_4^- \end{bmatrix} = \begin{bmatrix} -1 & 0 & k_1 & k_3 \\ 1 & 0 & k_5 & k_7 \\ 0 & -1 & f_1 & f_3 \\ 0 & 1 & f_5 & f_7 \end{bmatrix} \begin{bmatrix} V_1^+ \\ V_2^+ \\ V_3^+ \\ V_4^+ \end{bmatrix}, and$$

$$[s] = \begin{bmatrix} 1 & 0 & -k_2 & -k_4 \\ 1 & 0 & k_6 & k_8 \\ 0 & 1 & -f_2 & -f_4 \\ 0 & 1 & f_6 & f_8 \end{bmatrix}^{-1} \begin{bmatrix} -1 & 0 & k_1 & k_3 \\ 1 & 0 & k_5 & k_7 \\ 0 & -1 & f_1 & f_3 \\ 0 & 1 & f_5 & f_7 \end{bmatrix}$$

Hence,

$$S_{11} = \frac{(f_4 + f_8)(k_6 - k_2) + (f_2 + f_6)(k_4 - k_8)}{\Delta}$$

$$S_{12} = \frac{2(k_2k_8 - k_4k_6)}{\Delta}$$

$$S_{13} = \frac{(f_4 + f_8)(k_5k_2 - k_1k_6) + (f_2 + f_6)(k_1k_8 - k_5k_4) + (f_1 - f_5)(k_4k_6 - k_2k_8)}{\Delta}$$

$$S_{14} = \frac{(f_2 + f_6)(k_4k_7 + k_3k_8) - (f_4 + f_8)(k_2k_7 + k_3k_6) + (f_3 - f_7)(k_4k_6 - k_2k_8)}{\Delta}$$

and

$$S_{21} = \frac{2(f_4f_6 - f_2f_8)}{\Delta}$$

$$S_{22} = \frac{(k_2 + k_6)(f_8 - f_4) + (k_4 + k_8)(f_2 - f_6)}{\Delta}$$

$$S_{23} = \frac{(k_1 - k_5)(f_2f_8 - f_4f_6) - (k_2 + k_6)(f_4f_5 + f_1f_8) + (k_4 + k_8)(f_2f_5 + f_1f_6)}{\Delta}$$

$$S_{24} = \frac{(k_3 - k_7)(f_2f_8 - f_4f_6) - (k_2 + k_6)(f_4f_7 + f_3f_8) + (k_4 + k_8)(f_2f_7 + f_3f_6)}{\Delta}$$

$$S_{31} = \frac{-2(f_4 + f_8)}{\Delta}$$

$$S_{32} = \frac{2(k_4 + k_8)}{\Delta}$$

$$S_{33} = \frac{(f_4 + f_8)(k_1 - k_5) + (k_4 + k_8)(f_5 - f_1)}{\Delta}$$

$$S_{34} = \frac{(f_4 + f_8)(k_3 - k_7) + (k_4 + k_8)(f_7 - f_3)}{\Delta}$$

and

$$S_{41} = \frac{2(f_2 + f_6)}{\Delta}$$

$$S_{42} = \frac{-2(k_2 + k_6)}{\Delta}$$

$$S_{43} = \frac{(f_2 + f_6)(k_5 - k_1) + (k_2 + k_6)(f_1 - f_5)}{\Delta}$$

$$S_{44} = \frac{(f_2 + f_6)(k_7 - k_3) + (k_2 + k_6)(f_3 - f_7)}{\Delta}$$

Δ is defined as

$$\Rightarrow \Delta = (k_8 + k_4)(f_6 + f_2) - (k_6 + k_2)(f_4 + f_8)$$

Vita

姓名: 蔡坤宏

出生日期: 中華民國 70 年 6 月 26 日

學經歷:

國立板橋高級中學(85 年 9 月~88 年 6 月)

國立中央大學電機工程學系(88 年 9 月~92 年 6 月)

國立交通大學電子研究所碩士班(92 年 9 月~94 年 7 月)